

Dependence of related parameters on centrality and mass in a new treatment for transverse momentum spectra in high energy collisions

Pei-Pin Yang^{1,2,*}, Mai-Ying Duan^{1,2,†}, Fu-Hu Liu^{1,2,‡}

¹*Institute of Theoretical Physics & Department of Physics & State Key Laboratory of Quantum Optics and Quantum Optics Devices, Shanxi University, Taiyuan, Shanxi 030006, People's Republic of China*

²*Collaborative Innovation Center of Extreme Optics, Shanxi University, Taiyuan, Shanxi 030006, People's Republic of China*

Abstract: We collected the experimental data of transverse momentum spectra of identified particles produced in proton-proton (p - p), deuteron-gold (d -Au or d - A), gold-gold (Au-Au or A - A), proton-lead (p -Pb or p - A), and lead-lead (Pb-Pb or A - A) collisions measured by the ALICE, CMS, LHCb, NA49, NA61/SHINE, PHENIX, and STAR collaborations at different center-of-mass energies. The multisource thermal model at the quark level or the participant quark model is used to describe the experimental data. The free parameters, the effective temperature T , entropy index-related n , and revised index a_0 , in the revised Tsallis–Pareto-type function are extracted at the quark level. In most cases, T and n in central collisions are larger than those in peripheral collisions, and a_0 does not change in different centrality classes. With the increase in the mass of produced particle or participant quark, T and a_0 increase, and n does not change significantly. The behaviors of related parameters from p - p , p (d)- A , and A - A collisions are similar.

Keywords: Transverse momentum spectra, various particles, participant quark model, TP-like function

PACS: 12.40.Ee, 13.85.Hd, 24.10.Pa

1 Introduction

It is believed that quark-gluon plasma (QGP) is possibly generated in the environment of high temperature and high density formed within a few microseconds after the little Big Bang of high energy nucleus-nucleus (A - A) collisions [1, 2, 3, 4]. Then the collision system undergoes likely hydrodynamic evolution and finally many particles appear after the evolution. In the evolution, there are at least three main stages: initial, chemical freeze-out, and kinetic freeze-out. Different types of particles may experience different stages of evolution and then show different behaviors of distribution. In addition, different particles come from similar high energy collision process may have some similarities in their distributions [5, 6, 7, 8, 9, 10, 11, 12].

Quantum chromodynamics (QCD) is the fundamental theory of strong interactions in which quark and gluon are basic free particles. When the energy for ex-

changing gluons is very low, the confinement and chiral symmetry are restored. As a result, quark and gluon are almost massless. When the energy for exchanging gluons is very high, the confinement and chiral symmetry are destroyed, which gives quark rest mass. The characteristics of QGP are topics that people are more enthusiastic about [1, 2, 3, 4]. Recent studies have shown that QGP may be also formed in high-multiplicity events in high energy proton-proton (p - p) collisions [13]. Studying the transverse momentum spectra of various particles is one of the promising methods for learning the process of high energy collisions, and thus the nature of QGP can be understood. Studying the spectra in a wide range and with different centralities is an important method to further understand the mechanisms of QGP hadronization and particle production.

As we know, the calculation of hadron spectrum includes at least the quark potential model [14, 15] and the lattice QCD [16, 17, 18, 19, 20]. The former calculates

*E-mail: peipinyangshanxi@163.com; yangpeipin@qq.com

†E-mail: duanmaiying@sxu.edu.cn

‡Corresponding author. E-mail: fuhuliu@163.com; fuhuliu@sxu.edu.cn

the mass, width, and other properties of hadrons by constructing the interaction potential between quarks, and the latter studies the properties of hadrons mainly from the first principles. For the research of hadron's transverse momentum spectrum, people mainly study at the hadron level, except for a few at the quark level. In addition, the description of the larger transverse momentum (the transverse momentum being greater than 5 GeV/ c) is generally described by the multi-component distribution function. At least, the two-component distribution function is needed for wide spectra.

In the two-component function, the first component describes the spectrum in low transverse momentum region, which reflects the contribution of soft excitation process. The second component describes the spectrum in medium and high transverse momentum region, which reflects the contribution of hard scattering process. Due to the similarities in high energy collisions [5, 6, 7, 8, 9, 10, 11, 12], the soft and hard process may show similar characteristics such as the similar participant quarks. According to our studies [21, 22, 23] on the two-component function [23], we may think that the soft process is performed by the sea quarks and the hard process is performed by the valence quarks. It is possible that the contributions of soft and hard processes can be described by a unified function which reflects the contribution of participant quarks.

As a practicable method, we hope to use a simple function to systemize the wide spectra of various particles. In fact, in our recent work [21], in the framework of multisource thermal model at the quark level [22, 23] or participant quark model and based on the Tsallis statistics [24, 25, 26, 27, 28], we have used the convolution of two or three revised Tsallis–Pareto-type (TP-like) functions [29, 30, 31, 32] to fit the available spectra of various particles produced in p - p collisions at 200 GeV at the Relativistic Heavy Ion Collider (RHIC) and at 2.76 and 13 TeV at the Large Hadron Collider (LHC). The part behaviors of the considered convolution function are studied due to changing the main parameters which includes the effective temperature T , entropy index-related n , and revised index a_0 .

To see the behaviors of main parameters in the considered convolution function, we study the dependence of T , n , and a_0 on the event centrality C , the rest mass m_0 of produced particles, and the constituent mass m_q ($q = u, d, s, c, \text{ or } b$) of participant quarks in this paper. To compare conveniently, we collect i) the data on p - p collisions at 2.76, 5.02, and 7 TeV measured by the

ALICE [33, 34], CMS [35], and LHCb [36] Collaborations, respectively, ii) the data on deuteron-gold (d -Au or d -A) collisions at 200 GeV measured by the PHENIX collaboration [37, 38, 39, 40], iii) the data on gold-gold (Au-Au or A -A) collisions at 200 GeV measured by the PHENIX [37, 41, 39] and STAR [42, 43] Collaborations, iv) the data on proton-lead (p -Pb or p -A) collisions at 5.02 and 8.16 TeV measured by the ALICE collaboration [44, 45, 46, 47], and v) the data on lead-lead (Pb-Pb or A -A) collisions at 2.76 and 5.02 TeV measured by the ALICE collaboration [48, 34, 49, 50]. To test further, we also compare the convolution function with the data from p - p , Au-Au, and Pb-Pb collisions over a low energy range from 6.3 to 39 GeV.

The remainder of this paper is structured as follows. The formalism and method are shortly described in Section 2. Results and discussion are given in Section 3. In Section 4, we summarize our main observations and conclusions.

2 Formalism and method

Hadrons are composed of more basic components such as quarks. According to the multisource thermal model at the quark level [22, 23] or the participant quark model discussed in our recent work [21], we first assume that participant quark is isotropic in its rest frame, and hadron is contributed by participant quarks according to the combination. In the multisource thermal model, it is assumed that one, two, or more sources emit particles due to different generation mechanisms, source temperatures, and event samples. In a given event sample, particles with the same source temperature are generated by the same mechanism and are considered to be emitted from the same source. Participant quarks are considered to be the contributor quarks in the participant quark model.

In this article, we want to study the transverse momentum spectra with different centralities and larger transverse momentum range at the quark level. In our previous work [21], based on the Tsallis statistics [24, 25, 26, 27, 28], we revised the Tsallis–Pareto-type (TP-type) function [29, 30, 31, 32] to be the TP-like function. That is, we assume that the transverse momentum (p_T) spectrum of hadrons with rest mass m_0 satisfies the TP-like function,

$$f(p_T) = C_0 p_T^{a_0} \left(1 + \frac{\sqrt{p_T^2 + m_0^2} - m_0}{nT} \right)^{-n}. \quad (1)$$

Here the effective temperature T , entropy index-related n , and revised index a_0 are free parameters, and C_0 is the normalization constant related to free parameters. It should be noted that a_0 is a real number with non-dimension. Although the introduction of a_0 is a technical treatment only, it determines the bending degree of curve in low p_T region and then affects the slope of curve in medium and high p_T region due to the limitation of normalization. We have the dimensions of $p_T^{a_0}$ and C_0 to be $(\text{GeV}/c)^{a_0}$ and $(\text{GeV}/c)^{-a_0-1}$, respectively. Thus, the dimension of $C_0 p_T^{a_0}$ is $(\text{GeV}/c)^{-1}$ which is the same as the fit function.

In the combined quarks that form the hadron, the contribution of the i -th participant quark to the transverse momentum of hadron complies with

$$f_i(p_{ti}) = C_i p_{ti}^{a_0} \left(1 + \frac{\sqrt{p_{ti}^2 + m_{0i}^2} - m_{0i}}{nT} \right)^{-n}. \quad (2)$$

Here $f_i(p_{ti})$ is the probability density function of the transverse momentum p_{ti} contributed by the i -th participant quark, m_{0i} is the constituent mass of the i -th participant quark, and C_i is the normalization constant. A meson is a combination of two quarks, so $i = 1$ or 2 for mesons. A baryon is a combination of three quarks, so $i = 1, 2, \text{ or } 3$ for baryons. For tetraquark state, we have $i = 1, 2, 3, \text{ or } 4$. For pentaquark state, we have $i = 1, 2, 3, 4, \text{ or } 5$. For six-quark state, we have $i = 1, 2, 3, 4, 5, \text{ or } 6$. Equations (1) and (2) are essentially TP-like functions, but m_0 in Eq. (1) refers to the rest mass of the hadron described, and m_{0i} in Eq. (2) refers to the constituent mass of the i -th participant quark. If the i -th participant quark is q , we have $m_{0i} = m_q$.

Transverse momentum spectrum of mesons is the convolution of two TP-like functions, We have

$$\begin{aligned} f(p_T) &= \int_0^{p_T} f_1(p_{t1}) f_2(p_T - p_{t1}) dp_{t1} \\ &= \int_0^{p_T} f_2(p_{t2}) f_1(p_T - p_{t2}) dp_{t2}. \end{aligned} \quad (3)$$

Here $f_1(p_{t1})$ and $f_2(p_{t2})$ are the probability density functions of transverse momenta contributed by the first and second participant quarks, respectively, and $f(p_T)$ is the probability density function for p_T of mesons.

The transverse momentum spectrum of baryons is the convolution of three TP-like functions. The convolution of the first two TP-like function is:

$$\begin{aligned} f_{12}(p_{t12}) &= \int_0^{p_{t12}} f_1(p_{t1}) f_2(p_{t12} - p_{t1}) dp_{t1} \\ &= \int_0^{p_{t12}} f_2(p_{t2}) f_1(p_{t12} - p_{t2}) dp_{t2}. \end{aligned} \quad (4)$$

Here $f_{12}(p_{t12})$ is the probability density function of transverse momentum contributed by the first two participant quarks. After the first two TP-like functions are convoluted, they are convoluted with the third TP-like function:

$$\begin{aligned} f(p_T) &= \int_0^{p_T} f_{12}(p_{t12}) f_3(p_T - p_{t12}) dp_{t12} \\ &= \int_0^{p_T} f_3(p_{t3}) f_{12}(p_T - p_{t3}) dp_{t3}. \end{aligned} \quad (5)$$

Here $f(p_T)$ is the probability density function for p_T of baryons.

Equation (1) is used to describe the hadron spectra at the hadron level. Equations (3) and (5) are used to describe the meson and baryon spectra at the quark level, respectively. Although Eq. (1) is approximately successful in the fits of transverse momentum spectra of various particles in our recent work [21], we use Eqs. (3) and (5) in this paper to fit more accurately the transverse momentum spectra of hadrons at the quark level. In Eqs. (3)–(5), no matter how many participant quarks are considered, the number of parameters is always four which includes three free parameters and a normalization constant. That is to say that, we use the same parameters for different participant quarks in a given hadron.

3 Results and discussion

3.1 Comparison with data by Eqs. (3) and (5)

Figure 1(a) shows the p_T spectra, $(1/2\pi p_T) d^2 N / dp_T dy$, of different hadrons such as $\pi^+ + \pi^-$, $K^+ + K^-$, and $p + \bar{p}$ with pseudorapidity $|\eta| < 0.8$ and ϕ with rapidity $|y| < 0.5$ produced in inelastic (INEL) p - p collisions at 2.76 TeV, where N denotes the number of hadrons. The symbols represent the data measured by the ALICE Collaboration [33, 34] and the curves are our results fitted by Eq. (3) for mesons or (5) for baryons. Figure 1(b) shows the p_T spectra, $d\sigma / dp_T$, of prompt $\psi(2S)$ and $\psi(2S)$ from b with $2 < y < 4.5$ produced in INEL p - p collisions at 7 TeV and the p_T spectra, $Bd^2\sigma / dp_T dy$, of $\Upsilon(1S)$ with $|y| < 2.4$ produced in INEL p - p collisions at 5.02 TeV, where σ denotes the cross-section and B denotes the branch ratio. The symbols represent the data measured by the LHCb [36] and CMS [35] Collaborations respectively, and the curves are our results fitted by Eq. (3). Different symbols represent the spectra of different particles. Some of them are scaled by

multiplying different factors, as marked in the panels. The values of free parameters (T , n , and a_0), normalization constant (N_0 or σ_0), χ^2 , and number of degree of freedom (ndof) obtained from Eqs. (3) or (5) are listed in Table 1. The quark structures are also listed in Table 1. In the present fitting process and in the following

discussion, the constituent masses of various quarks and the rest masses of various hadrons are cited from “The Review of Particle Physics (2020)” [51]. One can see that the fit equation is in agreement with the data measured by the ALICE, CMS, and LHCb Collaborations at the LHC.

Table 1. Values of T , n , a_0 , N_0 (or σ_0), χ^2 , and ndof corresponding to the curves in Fig. 1, where the normalization constant σ_0 is for the cases of prompt $\psi(2S)$, $\psi(2S)$ from b , and $\Upsilon(1S)$ presented in Fig. 1(b). All the free parameters are extracted at the quark level.

Particle (quark structure)	T (GeV)	n	a_0	N_0 (σ_0 (nb))	χ^2/ndof
$\pi^+ + \pi^-$ ($u\bar{d}, d\bar{u}$)	0.216 ± 0.001	5.047 ± 0.023	-0.500 ± 0.004	4.102 ± 0.032	60/59
$K^+ + K^-$ ($u\bar{s}, s\bar{u}$)	0.203 ± 0.001	5.136 ± 0.023	-0.100 ± 0.003	0.483 ± 0.003	16/54
$p + \bar{p}$ ($uud, \bar{u}\bar{u}\bar{d}$)	0.205 ± 0.001	6.128 ± 0.020	-0.130 ± 0.002	$(5.176 \pm 0.063) \times 10^{-3}$	12/45
ϕ ($s\bar{s}$)	0.272 ± 0.001	5.362 ± 0.022	0.000 ± 0.002	$(4.490 \pm 0.054) \times 10^{-2}$	5/17
prompt $\psi(2S)$ ($c\bar{c}$)	0.538 ± 0.002	4.962 ± 0.023	0.300 ± 0.003	1439.485 ± 6.997	16/8
$\psi(2S)$ from b ($c\bar{c}$)	0.675 ± 0.001	5.135 ± 0.014	0.297 ± 0.002	244.885 ± 1.999	9/8
$\Upsilon(1S)$ ($b\bar{b}$)	0.668 ± 0.002	2.918 ± 0.021	0.297 ± 0.003	6.769 ± 0.047	5/2

Figure 2 shows the centrality dependent p_T spectra of (a) π^- , (b) π^+ , (c) K^- , (d) K^+ , (e) \bar{p} , (f) p , (g) π^0 , (h) $\phi \rightarrow K^+K^-$, (i) η , and (j) $J/\psi \rightarrow e^+e^-$ with $|\eta| < 0.35$ (or $|y| < 0.35$) produced in d -Au collisions at 200 GeV. The equation of p_T spectra for panels (a)–(f) and (h) is $(1/2\pi p_T)d^2N/dp_T dy$, for (g) and (i) is $(1/2\pi p_T N_{\text{evt}})d^2N/dp_T dy$, and for (j) is $(B/2\pi p_T)d^2N/dp_T dy$. Here N_{evt} denotes the number of events. Different symbols represent the experimental data with different centrality classes in d -Au collisions at 200 GeV, measured by the PHENIX Collaboration [37, 38, 39, 40]. As shown in the panels, some of them are scaled by multiplying different factors. The curves are our fitting results, which are approximately in agreement with the experimental data of d -Au collisions measured by the PHENIX Collaboration at the RHIC. The related parameters are listed in Table 2.

Similar with Fig. 2, Figure 3 shows the centrality dependent p_T spectra of (a) π^- , (b) π^+ , (c) K^- , (d) K^+ , (e) \bar{p} , (f) p , (g) π^0 , (h) $\phi \rightarrow K^+K^-$, (i) D^0 (\bar{D}^0), and (j) $J/\psi \rightarrow \mu^+\mu^-$ produced in Au-Au collisions at 200 GeV. The equation of p_T spectra for panels (a)–(f) and (h) is $(1/2\pi p_T)d^2N/dp_T dy$, for (g) and (i) is $(1/2\pi p_T N_{\text{evt}})d^2N/dp_T dy$, and for (j) is $(B/2\pi p_T)d^2N/dp_T dy$. The experimental data with given $|\eta|$ and $|y|$ ranges marked in the panels are measured by the PHENIX [37, 41, 39] and STAR [42, 43] Collaborations, respectively. Our fitting results, as

shown by the curves, are consistent with the experimental data of Au-Au collisions measured by the PHENIX and STAR Collaborations at the RHIC. See Table 3 for the fitting parameters.

Similar with Figs. 2 and 3, Figures 4(a)–4(e) show the centrality dependent p_T spectra, (a)–(c) $(1/2\pi p_T)d^2N/dp_T dy$ and (d) and (e) $(1/N_{\text{evt}})d^2N/dp_T dy$, of (a) $\pi^+ + \pi^-$, (b) $K^+ + K^-$, (c) $p + \bar{p}$, (d) $\Sigma(1385)^+$, and (e) $(\Xi(1530)^0 + \bar{\Xi}(1530)^0)/2$ with $-0.5 < y < 0$ measured by the ALICE Collaboration [44, 45] in p -Pb collisions at 5.02 TeV, accompanied by the p_T spectra of the mentioned particles in non-single diffraction (NSD) p - p collisions at the same energy per nucleon pair. Figure 4(f) shows the p_T spectra, $d^2N/dp_T dy$, of D^0 , D_s^+ , D^+ , and D^{*+} with $-0.96 < y < 0.04$, as well as $\Upsilon(1S)$ with $2.03 < y < 3.53$ and $-4.46 < y < -2.96$, measured by the ALICE Collaboration [46, 47] in minimum-bias (MB) p -Pb collisions at 5.02 and 8.16 TeV. The curves represent our fitted results and the related parameters are listed in Table 4. The fitting results are in agreement with the experimental data of p -Pb and p - p collisions measured by the ALICE Collaboration at the LHC.

Similar with Figs. 2, 3, and 4(a)–4(e), Figure 5 shows the transverse momentum spectra, (a)–(e) $(1/2\pi p_T)d^2N/dp_T dy$, (f) and (g) dN/dp_T , and (h) $d^2N/dp_T dy$, of (a) $\pi^+ + \pi^-$, (b) $K^+ + K^-$, (c) $p + \bar{p}$, (d) $(K^{*0} + \bar{K}^{*0})/2$, (e) ϕ , (f) D^+ (D^0), (g) D_s^+ (D^{*+}), and

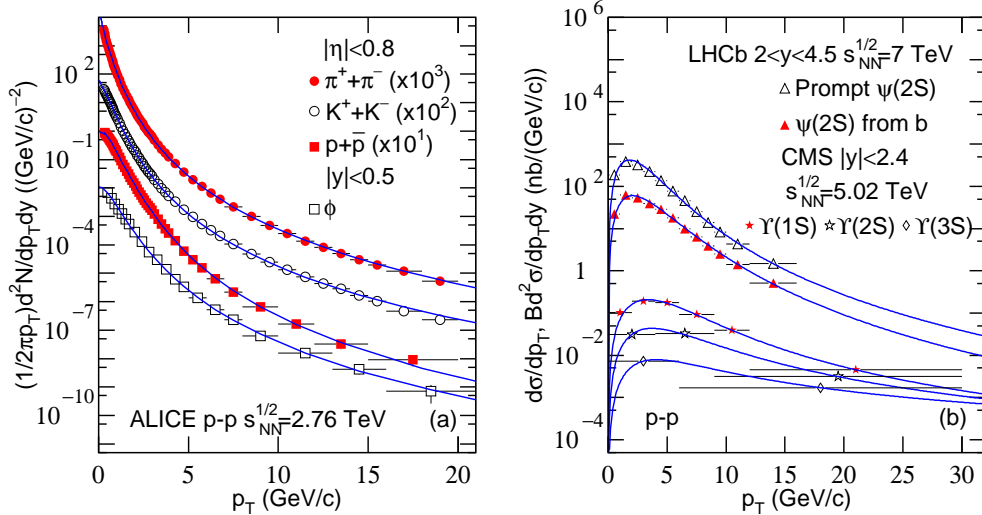


Figure 1: The transverse momentum spectra of different hadrons produced in INEL p - p collisions at $\sqrt{s_{\text{NN}}} = 2.76, 5.02,$ and 7 TeV, where $\sqrt{s_{\text{NN}}}$ ($s_{\text{NN}}^{1/2}$ in the panels) denotes the center-of-mass energy per nucleon pair and can be simplified to \sqrt{s} for p - p collisions. Different symbols represent the spectra of different particles measured by the ALICE [33, 34], CMS [35], and LHCb [36] Collaborations, where some of them are scaled by different factors marked in the panels. The curves are our fitted results by using Eqs. (3) for mesons and (5) for barons.

(h) inclusive J/ψ produced in Pb-Pb collisions at 2.76 TeV for panels (a)–(e) and 5.02 TeV for (f)–(h), with different $|\eta|$ or $|y|$ and centrality classes as marked in the panels. The symbols represent the experimental data measured by the ALICE Collaboration [48, 34, 49, 50]. The curves are our fitted results and the related parameters are listed in Table 5. The curves fit well with the experimental data measured by the ALICE Collaboration on Pb-Pb collisions at the LHC.

3.2 Dependence of parameters

We now analyze the dependences of effective temperature T , entropy index-related n , and revised index a_0 on centrality class C , rest mass m_0 of produced hadrons, and constituent mass m_q of participant quarks. The parameter values presented in the following discussions are cited from Tables 1–5 which are obtained from the fits to the experimental transverse momentum spectra displayed in Figs. 1–5.

Figure 6 shows the centrality dependence of parameter T extracted from the experimental data measured in (a) d -Au and (b) Au-Au collisions at the RHIC, as well as (c) p -Pb and (d) Pb-Pb collisions at the LHC, by international collaborations. One can see that the effec-

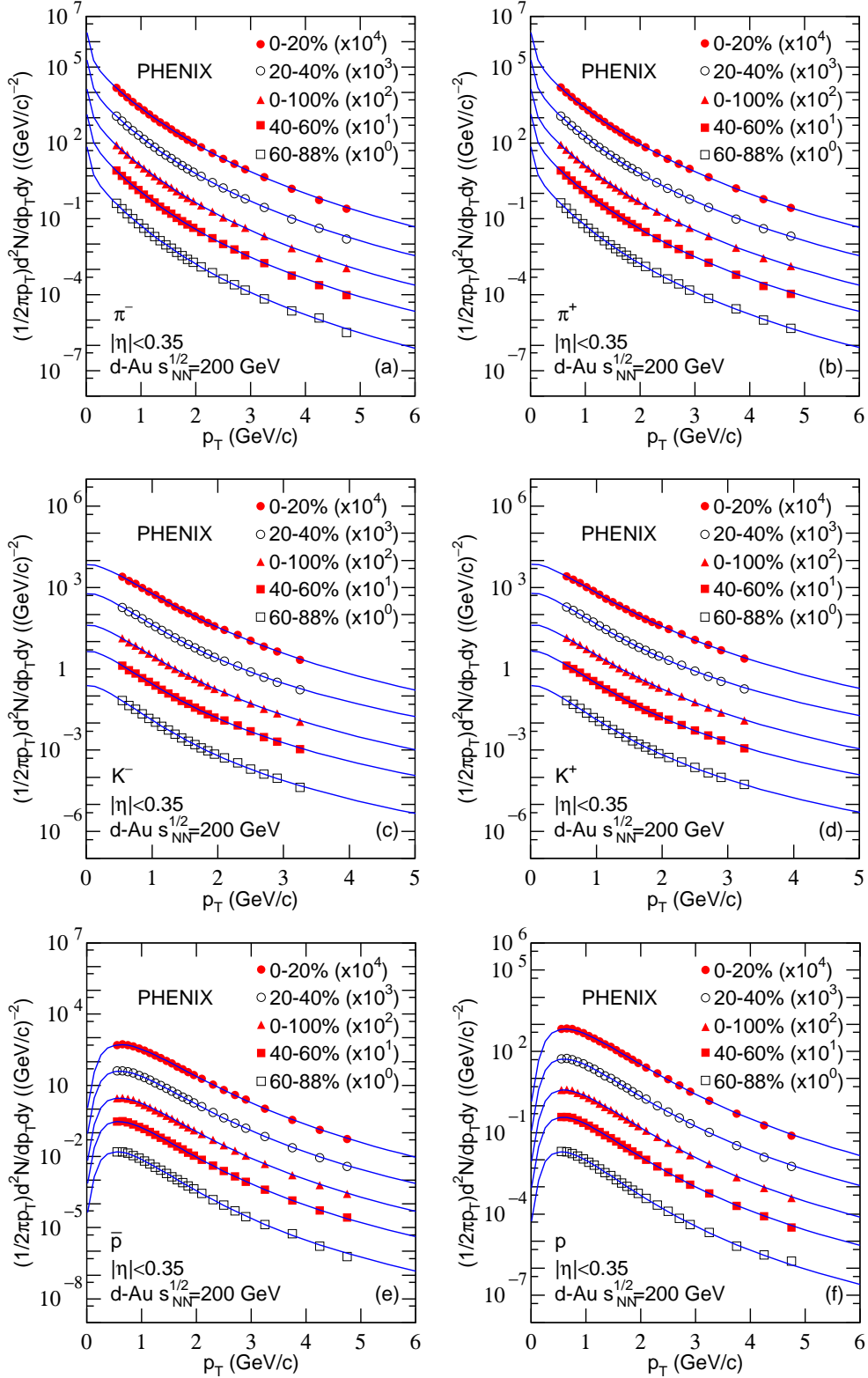
tive temperature of the emission source increases slowly with the increase of centrality from peripheral to central collisions in most cases. This renders that more collision energies are deposited in central collisions.

Figure 7 shows the dependence of parameter n on centrality C , where n is extracted from the experimental data under different conditions: (a) d -Au and (b) Au-Au collisions at the RHIC, as well as (c) p -Pb and (d) Pb-Pb collisions at the LHC. In the Tsallis statistics [24, 25, 26, 27, 28, 52], $n = 1/(q - 1)$, where q is the entropy index, refers to the equilibrium degree. Generally, $q = 1$ corresponds to an equilibrium state, and $q > 1$ corresponds to a non-equilibrium. One can see that n is very large and increases slowly with the increase of centrality from peripheral to central collisions, which means that q is close to 1 and further closes to 1 slowly with the increase of centrality. This study shows that the central collisions are closer to equilibrium state than the peripheral collisions. This situation is caused by more multiple scatterings in central collisions.

Now that we are talking about multiple scattering, we would like to point out that the multiple scattering at quark level in view of TP-like function used here differs from those at nucleonic level. At quark level, less multiple scatterings and elastic collisions should be happened due to very strong interactions among quark,

anti-quark, and gluon. At nucleonic level, more multiple scatterings and elastic collisions should be happened due to non-violent interactions between produced parti-

cle and nucleon. Both the multiple scatterings at quark and nucleonic levels lead to larger p_T and then wider spectra and larger T . Although the influence of multi-



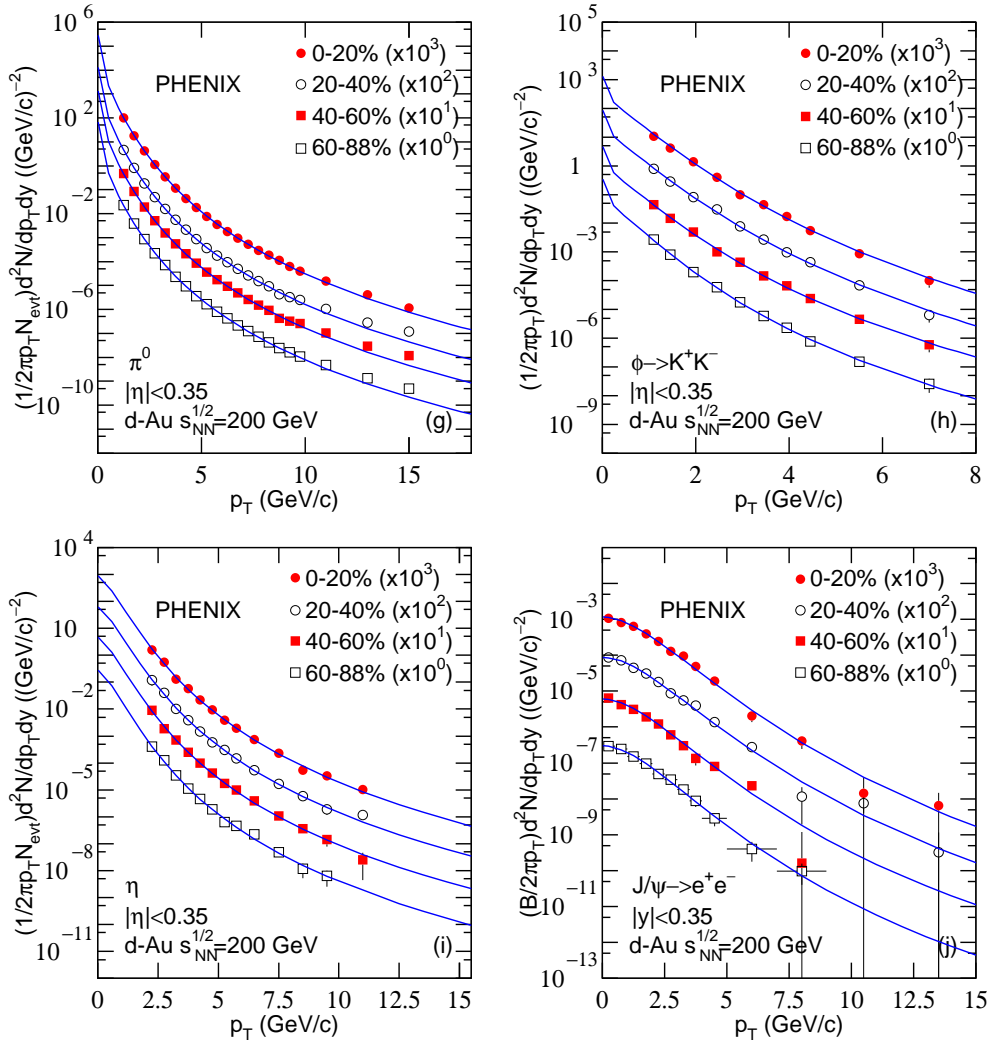


Figure 2: The transverse momentum spectra of (a) π^- , (b) π^+ , (c) K^- , (d) K^+ , (e) \bar{p} , (f) p , (g) π^0 , (h) $\phi \rightarrow K^+K^-$, (i) η , and (j) $J/\psi \rightarrow e^+e^-$ with (a)–(i) $|\eta| < 0.35$ (or (j) $|y| < 0.35$) in different centrality classes produced in d -Au collisions at 200 GeV. Different symbols represent different centrality classes measured by the PHENIX Collaboration [37, 38, 39, 40]. Some of them are scaled by different factors marked in the panels. The curves are our fitted results by using Eqs. (3) for mesons and (5) for baryons.

ple scattering at quark level is less than that at nucleonic level, the final effect is the sum of two types of multiple scatterings.

From Tables 2–5 one can see that, for given particle and collisions, the parameter a_0 is independent of centrality C . So we have not displayed the figure about the dependence of parameter a_0 on centrality C to avoid trivialness. As a parameter that characterizes the bending degree of the function curve in the low p_T region, the fact that a_0 is independent of C implies that the spectator does not affect the production of particles with low p_T . Meanwhile, the size of participant region does not affect the production at low p_T , too. The production at

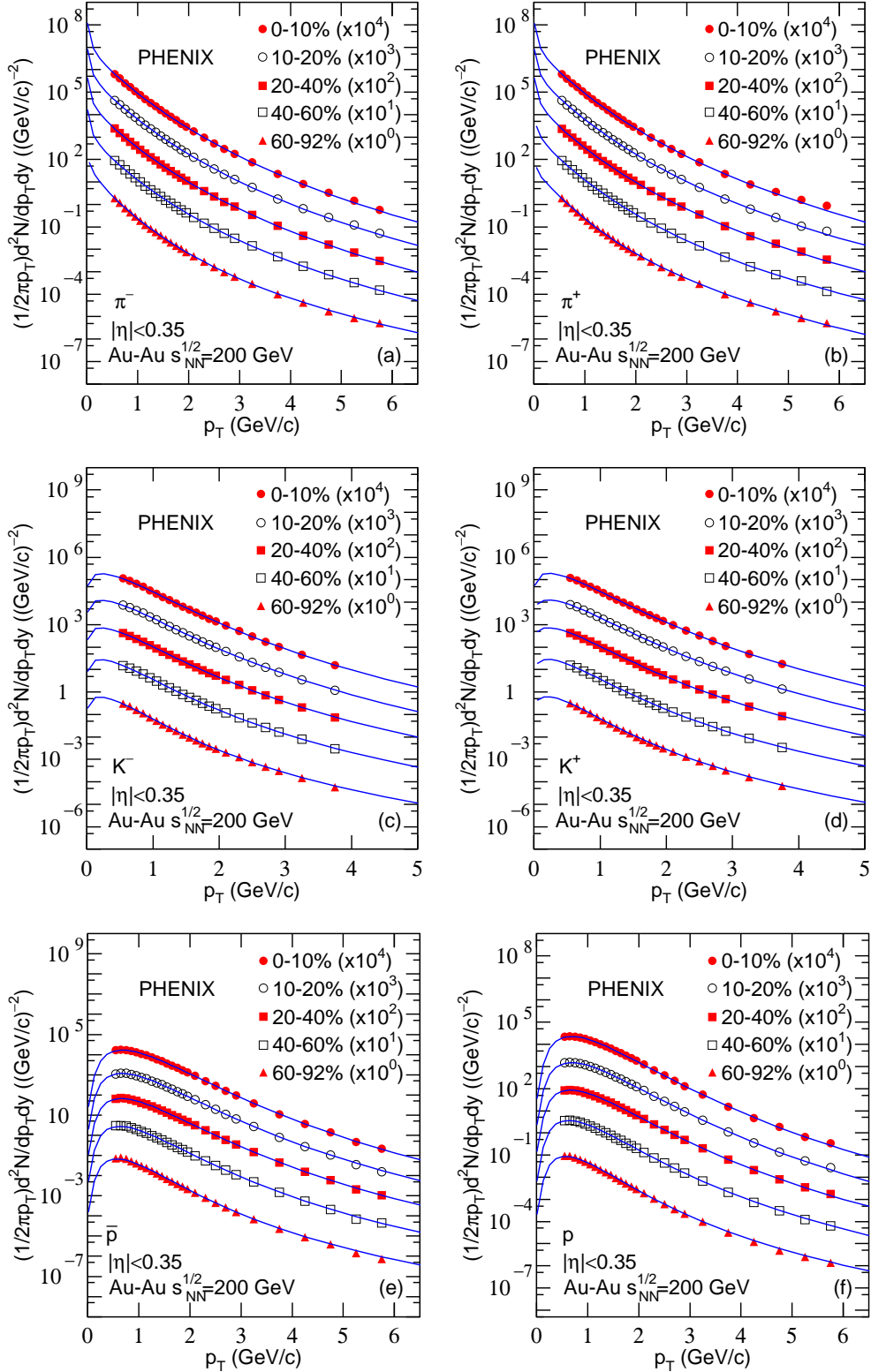
low p_T is mainly determined by the individual nucleon-nucleon collision or two or three participant quarks.

Figures 8, 9, and 10 show the trends of parameters T , n , and a_0 with the rest mass m_0 of corresponding hadron, respectively. In the three figures, panels (a)–(e) correspond to the results of p - p , d -Au, Au-Au, p -Pb, and Pb-Pb collisions, respectively. The results for various centrality classes in nuclear collisions are displayed together without distinction. In Fig. 8, the effective temperature T is positively correlated with the rest mass of hadron. This means that the massive hadrons are produced at a higher temperature. In Figs. 9(b) and 9(c), due to the small range of rest mass of hadron, the

parameter n has no obvious dependence on rest mass of hadron. In Figs. 9(a), 9(d), and 9(e), one can see that the entropy index-related n decreases with the increase of rest mass of hadron. One can observe from Fig. 10

that as the rest mass of hadron increases, the revised index a_0 tends to increase.

It is not easy to observe the trend of parameters with the constituent quark mass m_q of corresponding



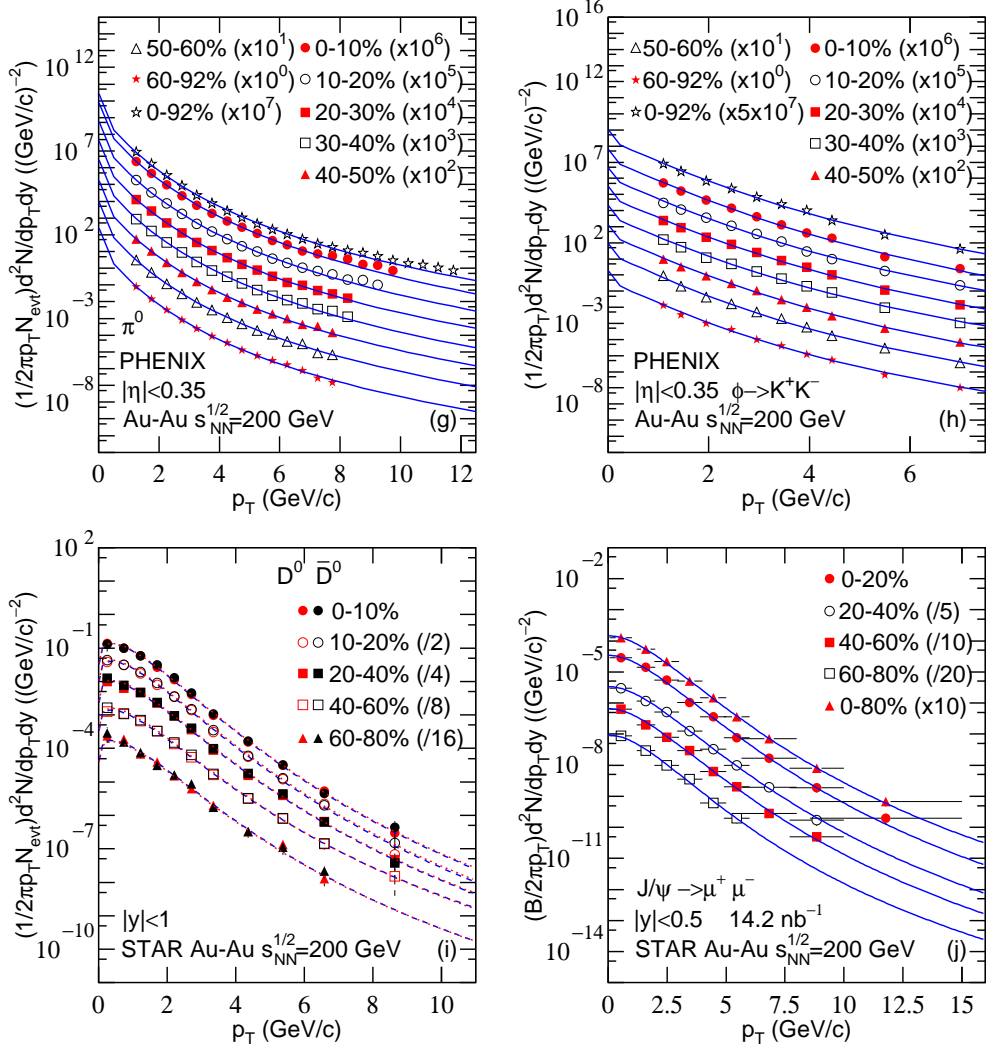


Figure 3: The transverse momentum spectra of (a) π^- , (b) π^+ , (c) K^- , (d) K^+ , (e) \bar{p} , (f) p , (g) π^0 , (h) $\phi \rightarrow K^+K^-$, (i) D^0 (\bar{D}^0), and (j) $J/\psi \rightarrow \mu^+\mu^-$ with mid- η or mid- y produced in Au-Au collisions at 200 GeV. Different symbols represent different centrality classes measured by (a)–(h) the PHENIX Collaboration [37, 39, 41] and (i)–(j) the STAR Collaboration [42, 43]. Some of them are scaled by different factors marked in the panel. The curves are our fitted results by using Eqs. (3) for mesons and (5) for baryons, where the dotted and dashed curves fit the spectra of D^0 and \bar{D}^0 respectively.

hadron in Tables 1–5. In order to observe it more intuitively, Figures 11, 12, and 13 show the dependences of parameters T , n , and a_0 on the constituent quark mass m_q of corresponding hadron, respectively. In the three figures, panels (a)–(e) correspond to the results of p - p , d -Au, Au-Au, p -Pb, and Pb-Pb collisions, respectively. The results for various centrality classes in nuclear collisions are displayed together without distinction. One can clearly see that the correlation trend of parameters with constituent quark mass of hadron is consistent with that of parameters with rest mass of hadron. The parameters T and a_0 are positively correlated with the

constituent quark mass m_q . In Figs. 12(b) and 12(c), there is no obvious change trend being observed due to the small constituent quark mass range. In Figs. 12(a), 12(d), and 12(e), the parameter n has a negative correlation with the constituent quark mass. It should be pointed out that we have used the same symbol for the parameter points of different quarks in the same hadron.

3.3 More discussions

The trends of parameters T , n , and a_0 with the rest mass m_0 of hadrons and with the constituent mass m_q of quarks are the same correspondingly. This phenomenon

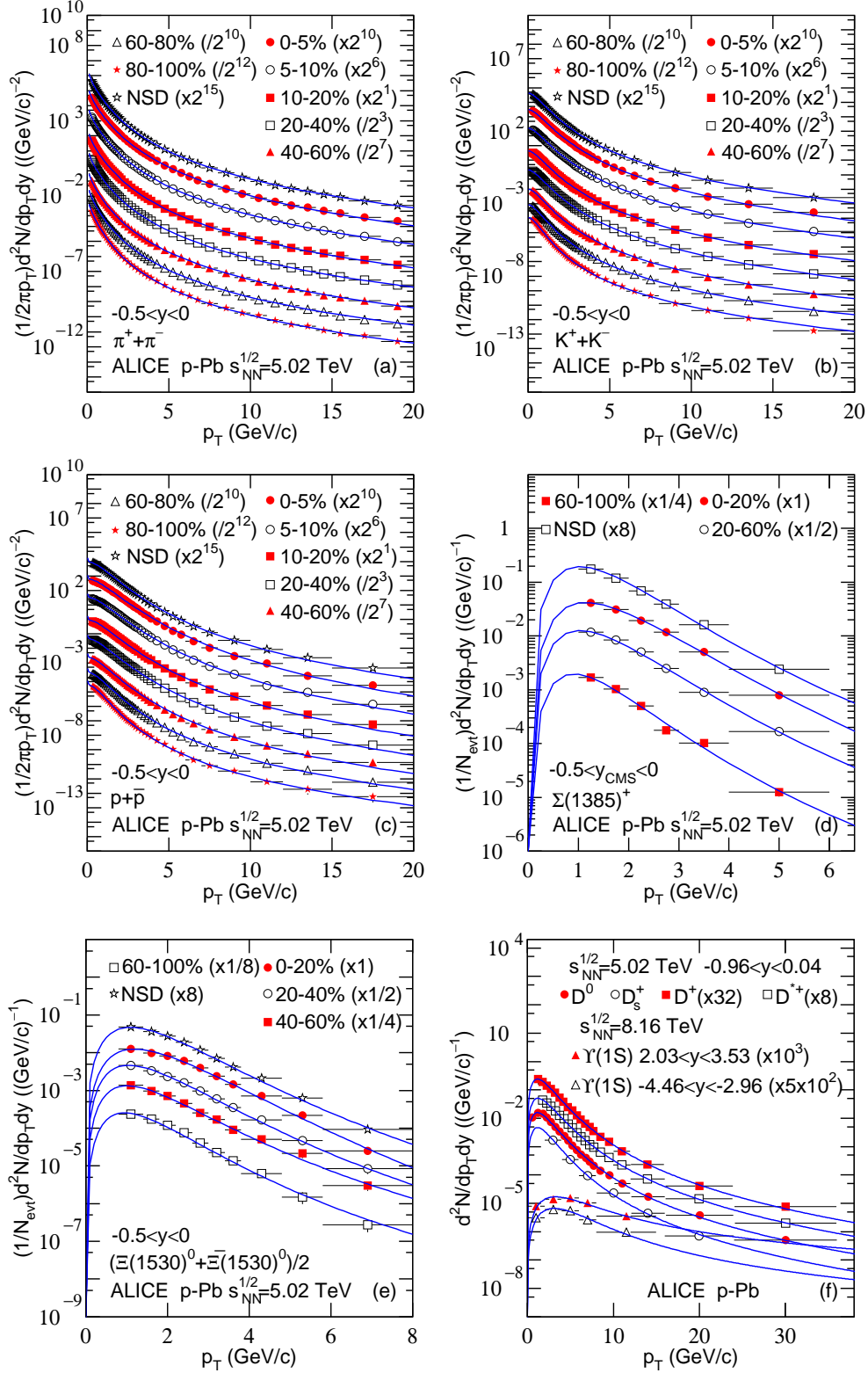


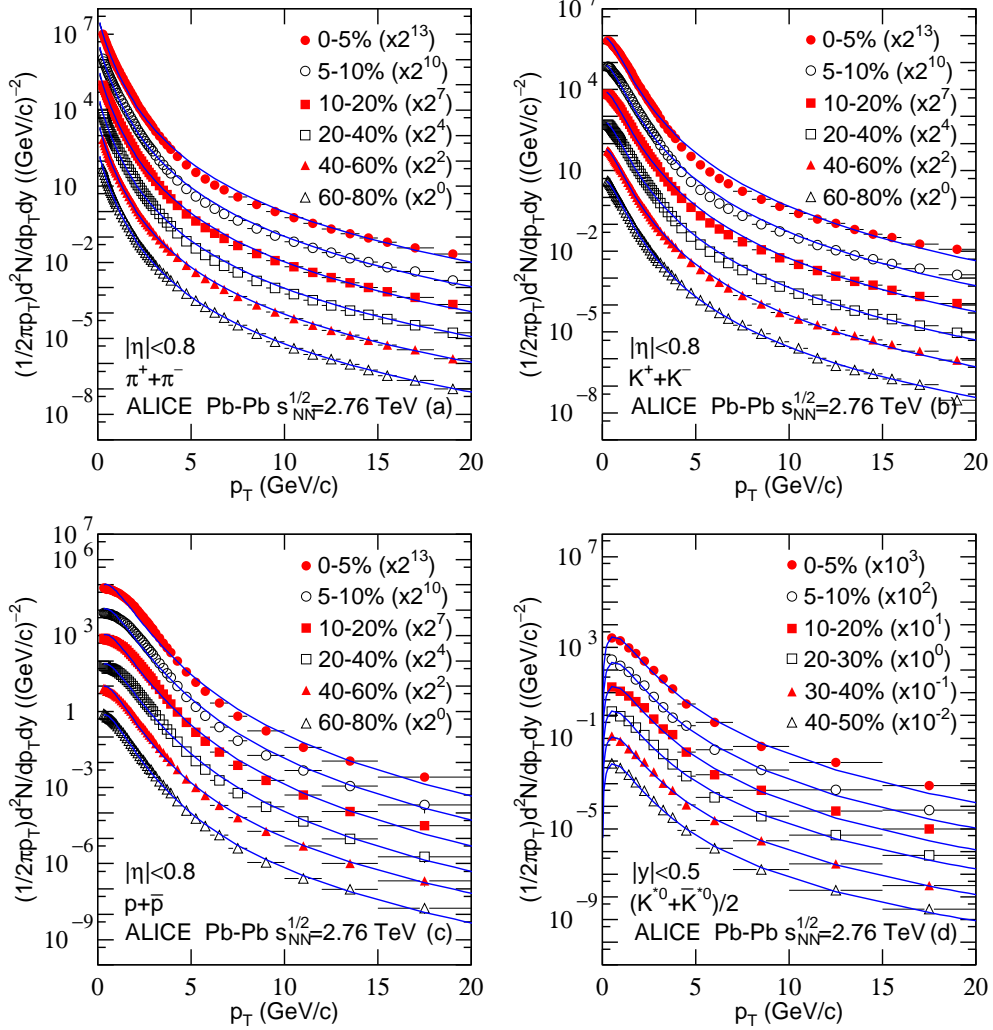
Figure 4: The transverse momentum spectra of (a) $\pi^+ + \pi^-$, (b) $K^+ + K^-$, (c) $p + \bar{p}$, (d) $\Sigma(1385)^+$, and (e) $(\Xi(1530)^0 + \bar{\Xi}(1530)^0)/2$ with $-0.5 < y < 0$ in different centrality p-Pb and NSD p-p collisions at 5.02 TeV, as well as of (f) D^0 , D_s^+ , D^+ , and D^{*+} with $-0.96 < y < 0.04$, as well as $\Upsilon(1S)$ with $2.03 < y < 3.53$ and $-4.46 < y < -2.96$, in MB p-Pb collisions at 5.02 and 8.16 TeV. Different symbols represent the experimental data in different cases measured by the ALICE Collaboration [44, 45, 46, 47]. Some of them are scaled by different factors marked in the panel. The curves are our fitted results by using Eqs. (3) for mesons and (5) for baryons.

can be explained as follows: the heavy hadrons are composed of heavy flavor quarks with larger constituent mass, while the light hadrons correspond to light flavor quarks with smaller constituent mass. The values of effective temperature T increase with the increase of mass (rest mass of hadron or constituent mass of quarks), which can be interpreted as the higher temperature is required for the production of massive particles. The parameter n decreases with the increase of mass. This means that the heavier hadron corresponds to the further away state from the equilibrium, though the system is still close to the equilibrium.

Although there have existed a big number of publications which went deeper in the transverse momentum spectra [25, 53, 54, 55, 56, 57, 58, 59, 60, 61, 62, 63, 64, 65, 66, 67, 68], especially for the analysis on the dependence of related parameters on centrality and mass, we have applied another unique Tsallis model to study

the mentioned spectra. In our treatment, for the model itself, different participant quark for given particle has the same form of probability density function with the same value of parameter. However, it was proposed to contribute to the transverse momentum differently due to different mass. This mass dependent transverse momentum spectrum is a natural result.

Comparing with the fits of Tsallis-inspired models (not exactly the same model) in other publications [25, 53, 54, 55, 56, 57, 58, 59, 60, 61, 62, 63, 64, 65, 66, 67, 68], the present work studies the spectra at the quark level and uses a more flexible treatment for the spectra in very low transverse momentum region. The related spectra studied in other publications can also be fitted by the present model. In fact, not only for the spectra with exponential form in low transverse momentum region but also for the spectra with inverse power-law form (from perturbative QCD) in medium and high transverse mo-



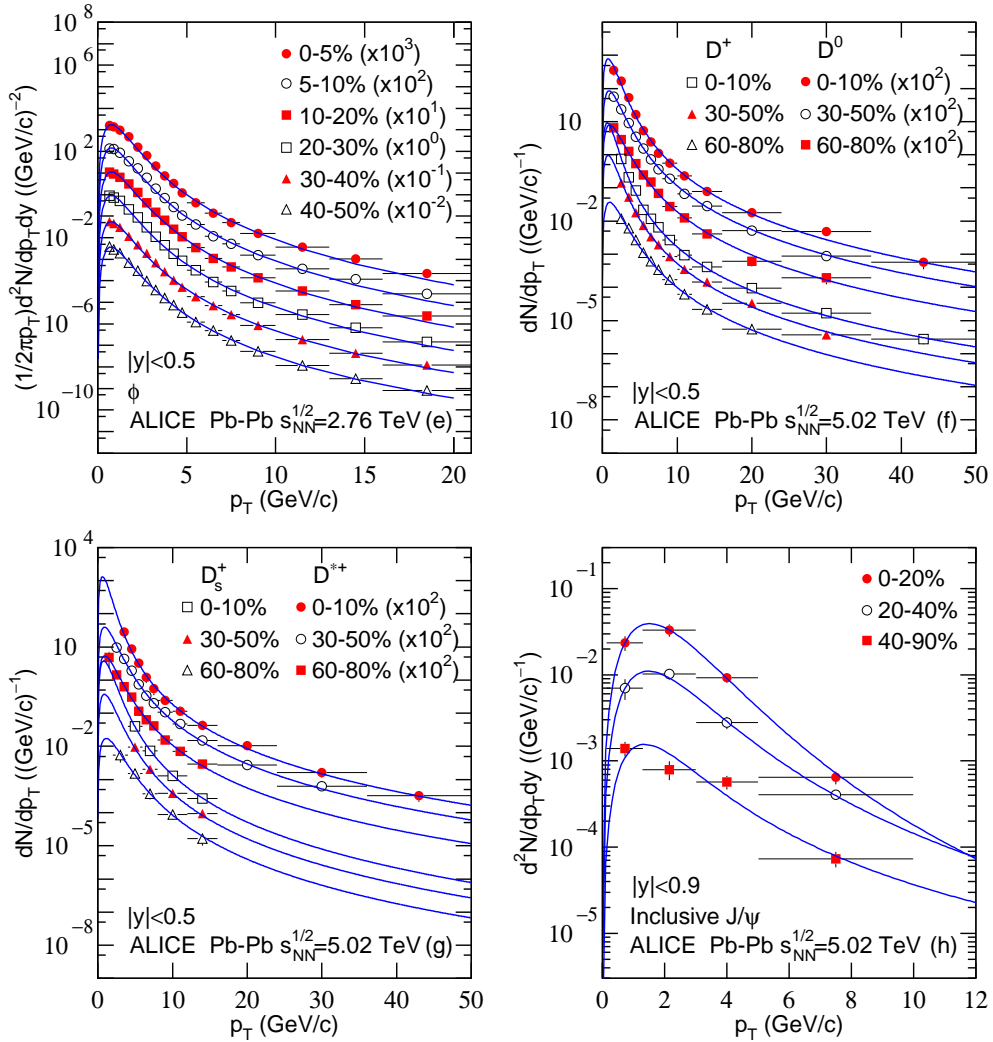


Figure 5: The transverse momentum spectra of (a) $\pi^+ + \pi^-$, (b) $K^+ + K^-$, (c) $p + \bar{p}$, (d) $(K^{*0} + \bar{K}^{*0})/2$, (e) ϕ , (f) D^+ (D^0), (g) D_s^+ (D^{*+}), and (h) inclusive J/ψ produced in Pb-Pb collisions at (a)–(e) 2.76 TeV and (f)–(h) 5.02 TeV with different $|\eta|$ or $|y|$ and centrality classes. The symbols represent the experimental data measured by the ALICE Collaboration [48, 34, 49, 50]. Some of them are scaled by different factors. The curves are our fitted results by using Eqs. (3) for mesons and (5) for baryons.

momentum region, the present model can fit different spectra flexibly [21]. Even for the spectra of jets, the present model can be used approximately [69].

There is connection between Eq. (1) and the well known inverse power-law or the Hagedorn function which is empirically inspired by perturbative QCD [70, 71]. Let $a_0 = 1$ and at high p_T (i.e. neglect m_0) in Eq. (1), we have $f(p_T) = C_0 p_T (1 + p_T/nT)^{-n}$, which is the inverse power-law or the Hagedorn function. Here T , n , and C_0 are different from those in Eq. (1) due to the refit and normalization. If we use $n = 1/(q-1)$, a different q from the above discussion can be obtained. This simplification results in the meanings of parameters in

Eq. (1) to be more obvious. Meanwhile, Eq. (1) also has a more solid foundation. To fit the spectra better, the inverse power-law or Hagedorn function has been revised by at least three forms [39, 72, 73, 74, 76, 77, 78], which is beyond the focus of the present work and will not be discussed anymore.

In the model, although the effective temperature T in the function is possibly not the physical temperature exactly, its physical significance is obvious. In fact, T reflects the average kinetic energy of considered quarks. Generally, T contains the contributions of thermal motion and collective flow [79]. Only the former contributes to the physical temperature. In the process of partici-

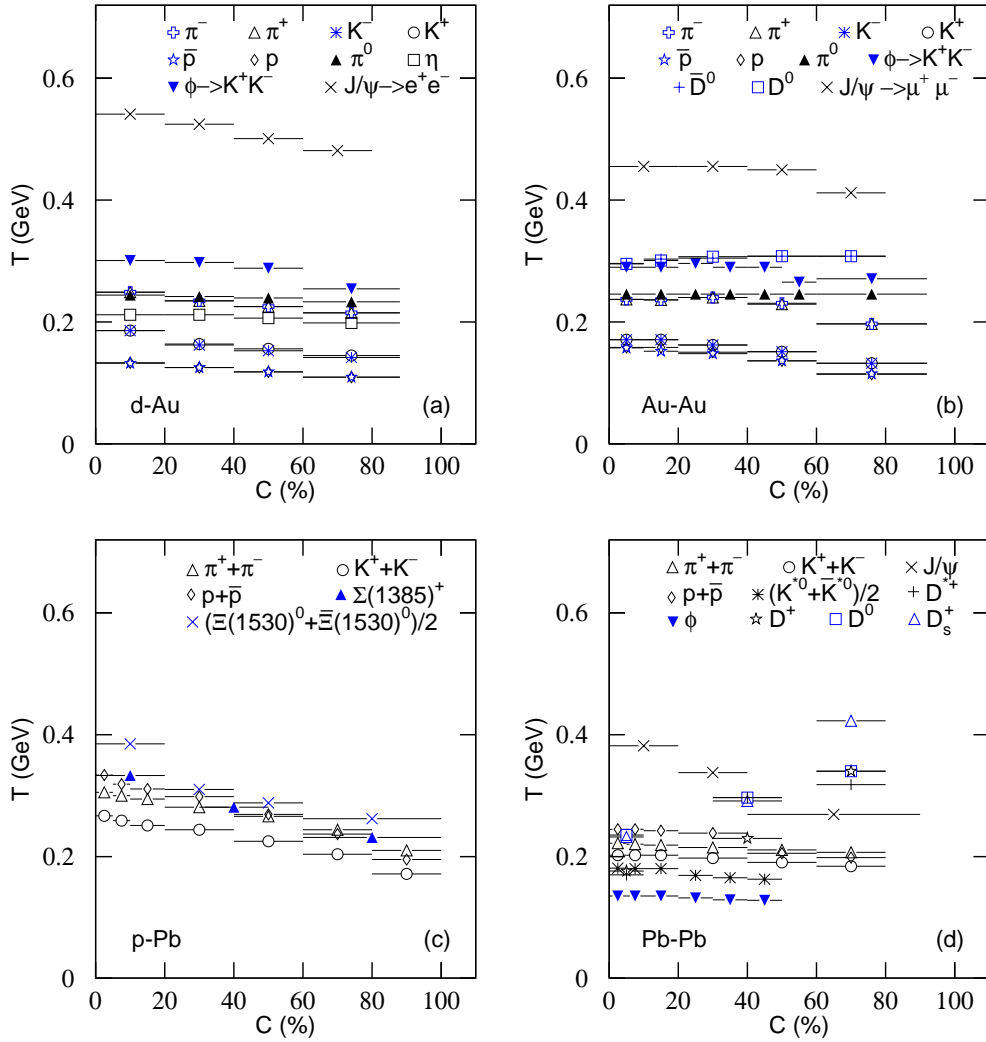


Figure 6: Dependence of effective temperature T on centrality C in (a) d -Au, (b) Au-Au, (c) p -Pb, and (d) Pb-Pb collisions at the RHIC or LHC. The obtained values of parameter T corresponding to identified particles are extracted from the experimental transverse momentum spectra and listed in Tables 2–5.

part quarks taking part in the microscopic collisions, the collective flow has not yet formed because the macroscopic squeeze and expansion of the collision system is delayed to show the flow effect. So, as a quantity extracted at the quark level, T is mainly contributed by the thermal motion. In other words, we may regard T as the physical temperature approximately.

The value of T extracted at the quark level is obviously larger than the critical temperature (≈ 0.16 GeV) of chemical freeze-out. There are two reasons causing this difference. On the one hand, T contains the contribution of flow effect which increases T [79]. On the other hand, T extracted at the quark level describes the earlier collision system which stays at higher excitation state with higher temperature than the stage of chemical

freeze-out. Besides, different models use different temperature parameters which can be fitted (“measured”) by different functions (“thermometers”). So, the difference between T and critical temperature is natural. Of course, a unified “thermometer” is needed in high energy collisions. This issue is beyond the focus of the present work and we will not discuss it anymore.

It is possible to quantify the thermal and collective part of the hadron spectra in terms of the parameters extracted. In fact, in our previous works [80, 81, 82, 83, 84, 85], the intercept in the relation of effective temperature versus rest mass of hadron is regarded as the physics temperature of emission source at the stage of kinetic freeze-out. The slope in the relation of average transverse momentum versus average energy of hadron

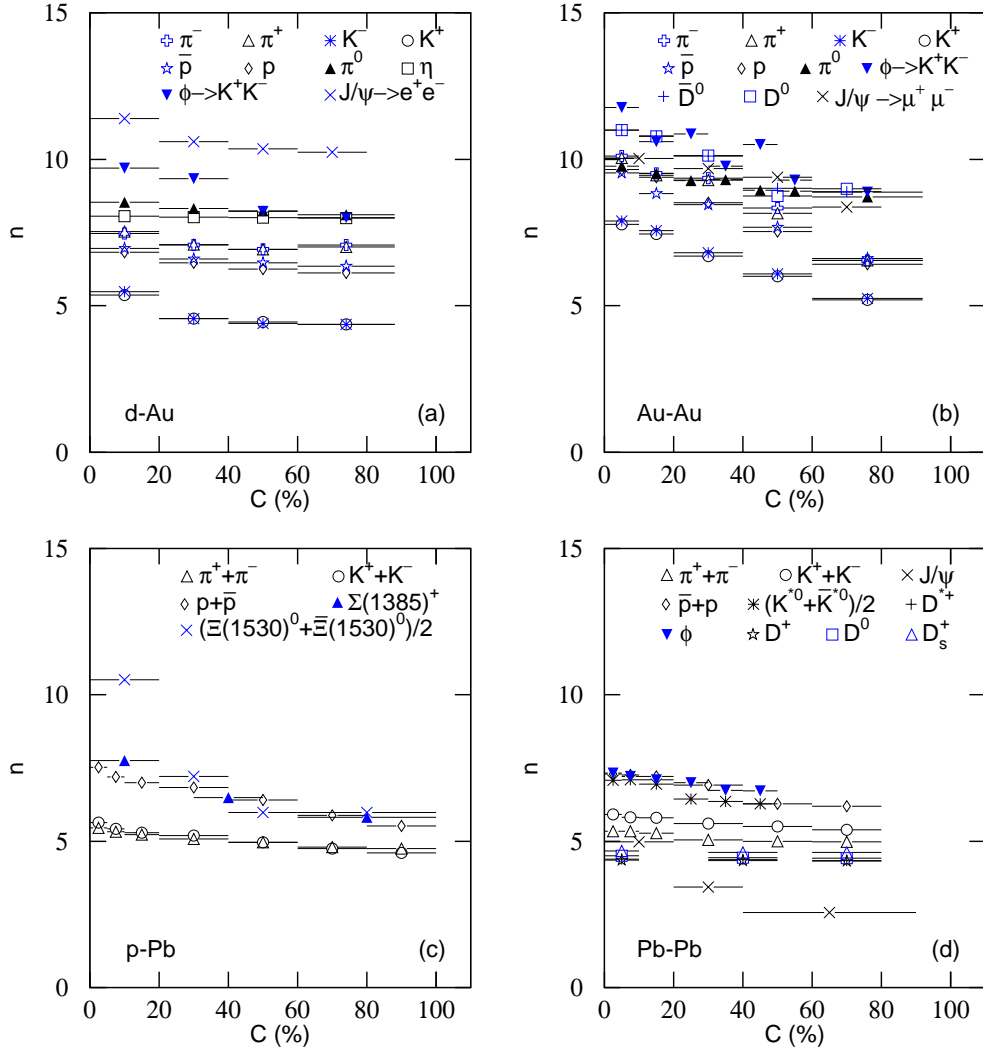


Figure 7: Dependence of parameter n on centrality C in (a) d -Au, (b) Au-Au, (c) p -Pb, and (d) Pb-Pb collisions at the RHIC or LHC. The obtained parameter values corresponding to identified particles are cited from Tables 2–5.

in the source rest frame is regarded as the transverse flow velocity. According to the obtained parameters, we may calculate the average transverse momentum and average energy, and obtain the physics temperature and transverse flow velocity. Based on the mentioned method of intercept and slope, we have quantified the thermal and collective part in our previous works [80, 81, 82, 83, 84, 85] at the hadronic level.

Compared to the Tsallis and Hagedorn descriptions, the present work presents a more accurate description of the transverse momentum spectra in wider range and for more particles. At the quark level, we should consider to use the quantities related to quark to quantify the thermal and collective part. Based on our experience, at least three types of quarks, $u(d)$, s , and c , are needed.

More quarks may possibly result in the mass-dependent differential kinetic freeze-out scenario [82]. At the top RHIC or LHC energy, for symmetric INEL p - p and central A - A collisions, the physics temperature estimated by us increases from 0.12 to 0.19 GeV with the increase of system size due to more energy deposition in large system. The transverse flow velocity decreases from 0.10 to 0.05 c with the increase of system size due to large stopping of medium for quarks in large system.

The Tsallis non-extensive entropy parameter q or the entropy index-related n is related to equilibrium degree. In most cases, when the collision system emits light and heavy hadrons, q is close to 1 or n is large. This means that the collision system at the RHIC and LHC stays in an approximate equilibrium state. In fact, when the

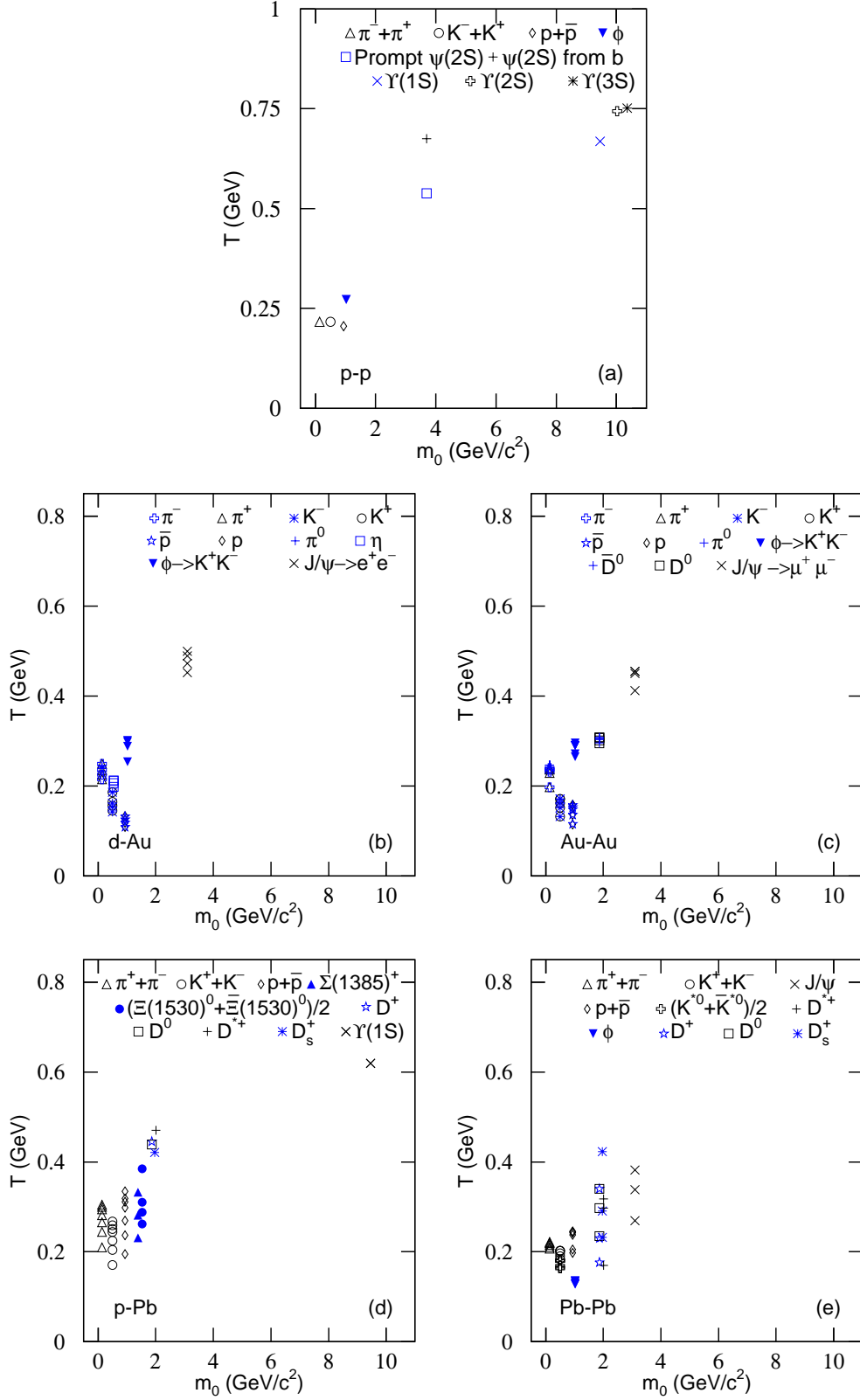


Figure 8: Dependence of effective temperature T on rest mass m_0 of hadrons produced in (a) p - p , (b) d -Au, (c) Au-Au, (d) p -Pb, and (e) Pb-Pb collisions at the RHIC or LHC. The obtained values of parameter T corresponding to identified particles are extracted from the experimental transverse momentum spectra and listed in Tables 1–5. The free parameter is extracted at the quark level, though the dependence of free parameter on rest mass of hadron is given.

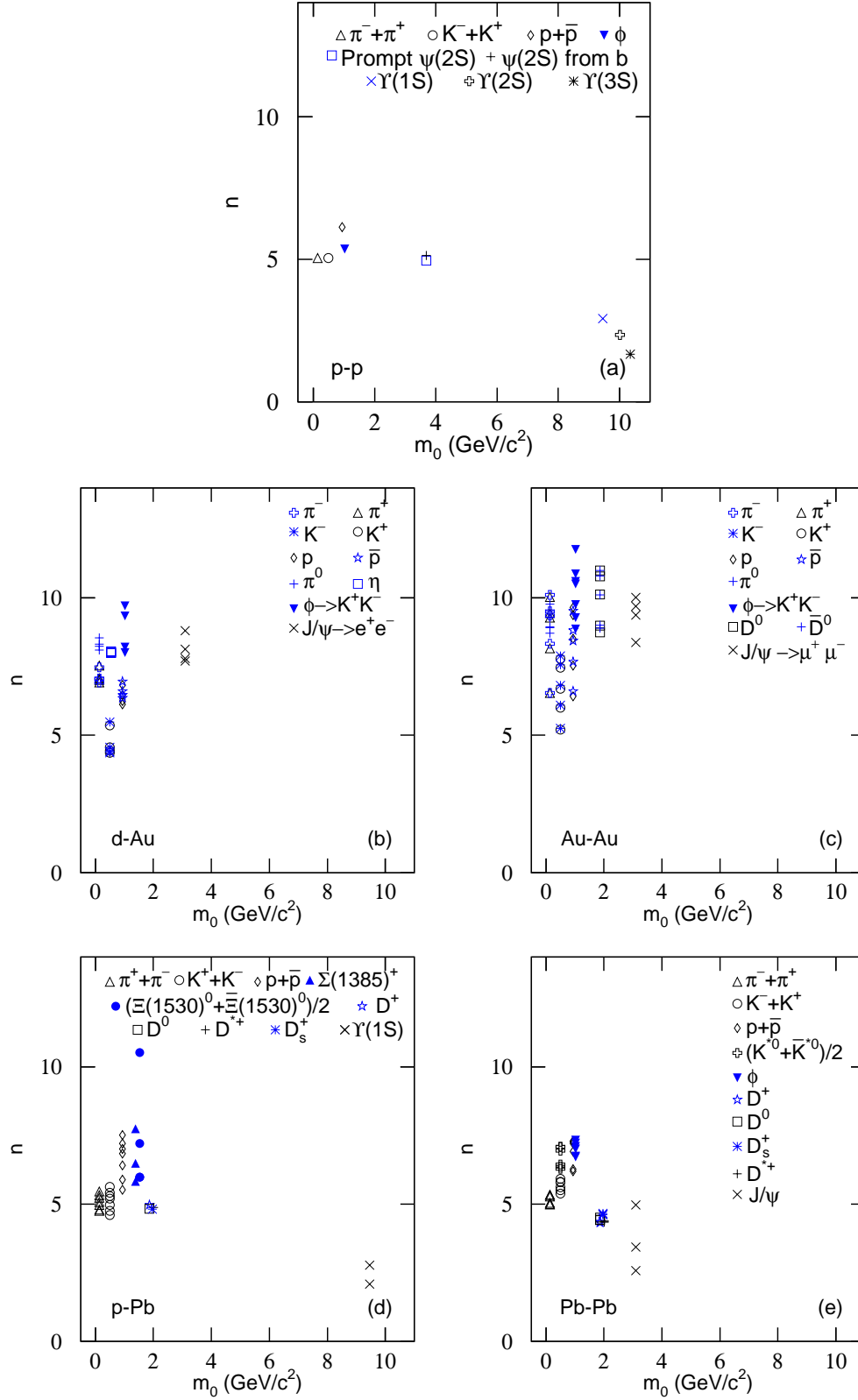


Figure 9: Dependence of parameter n on rest mass m_0 of hadrons in (a) p - p , (b) d -Au, (c) Au-Au, (d) p -Pb, and (e) Pb-Pb collisions at the RHIC or LHC. The obtained parameter values corresponding to identified particles are cited from Tables 1–5. The free parameter is extracted at the quark level, though the dependence of free parameter on rest mass of hadron is given.

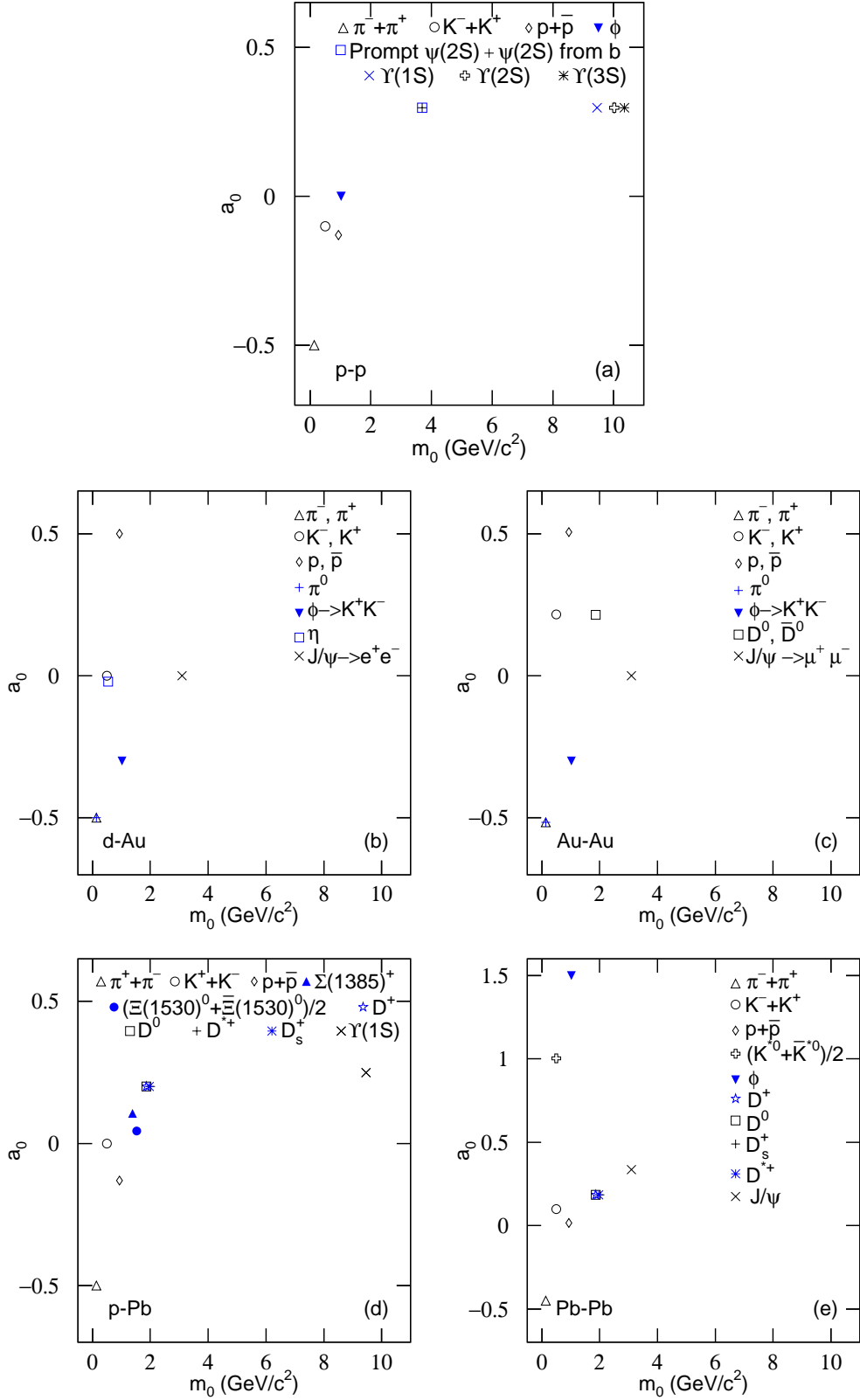


Figure 10: Dependence of parameter a_0 on rest mass m_0 of hadrons in (a) p - p , (b) d -Au, (c) Au-Au, (d) p -Pb, and (e) Pb-Pb collisions at the RHIC or LHC. The obtained parameter values corresponding to identified particles are cited from Tables 1–5. The free parameter is extracted at the quark level, though the dependence of free parameter on rest mass of hadron is given.

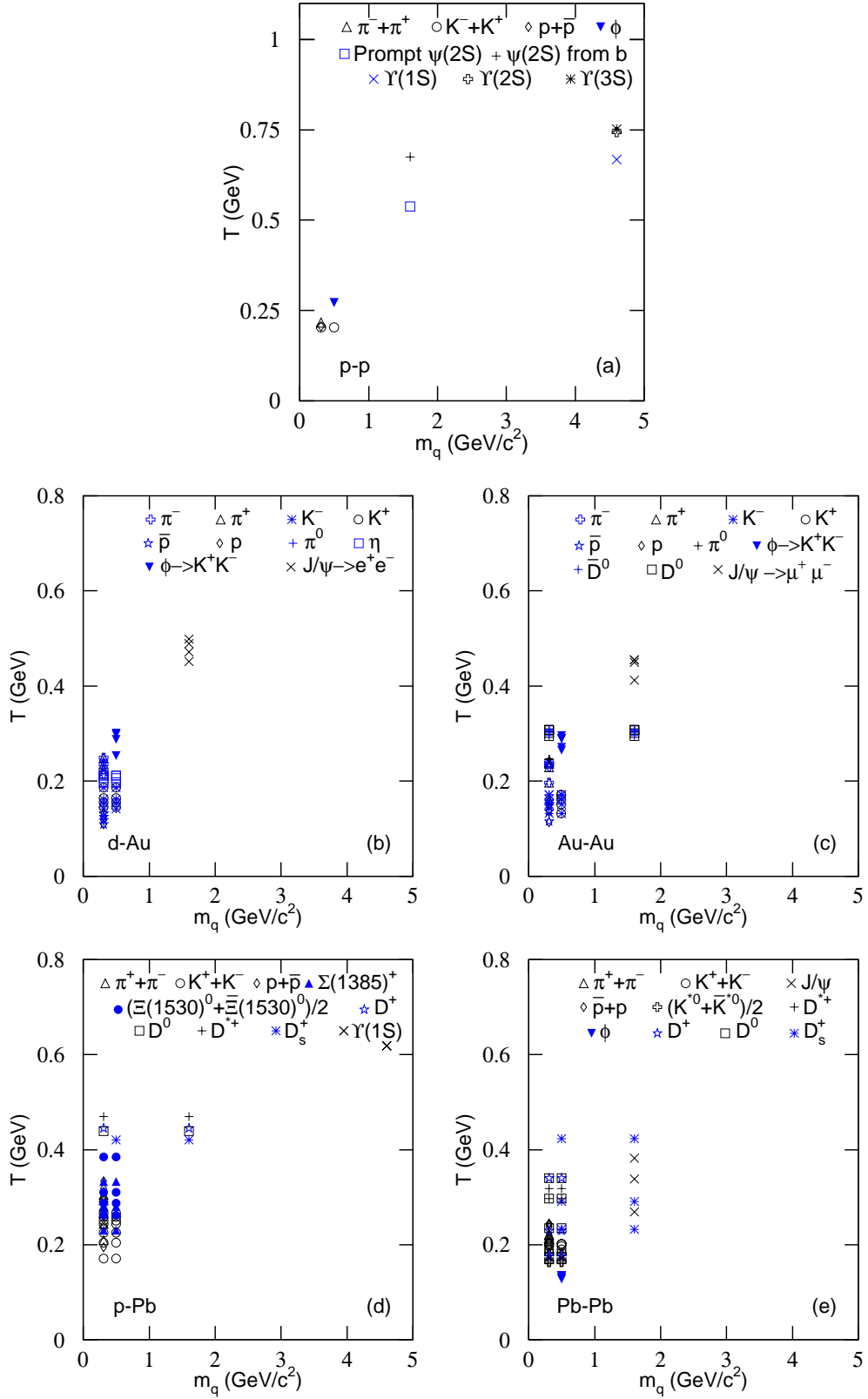


Figure 11: Dependence of effective temperature T on constituent mass m_q of quarks that make up hadrons produced in (a) p - p , (b) d -Au, (c) Au-Au, (d) p -Pb, and (e) Pb-Pb collisions at the RHIC or LHC. The obtained values of parameter a_0 corresponding to various quarks are extracted from the experimental transverse momentum spectra and listed in Tables 1–5.

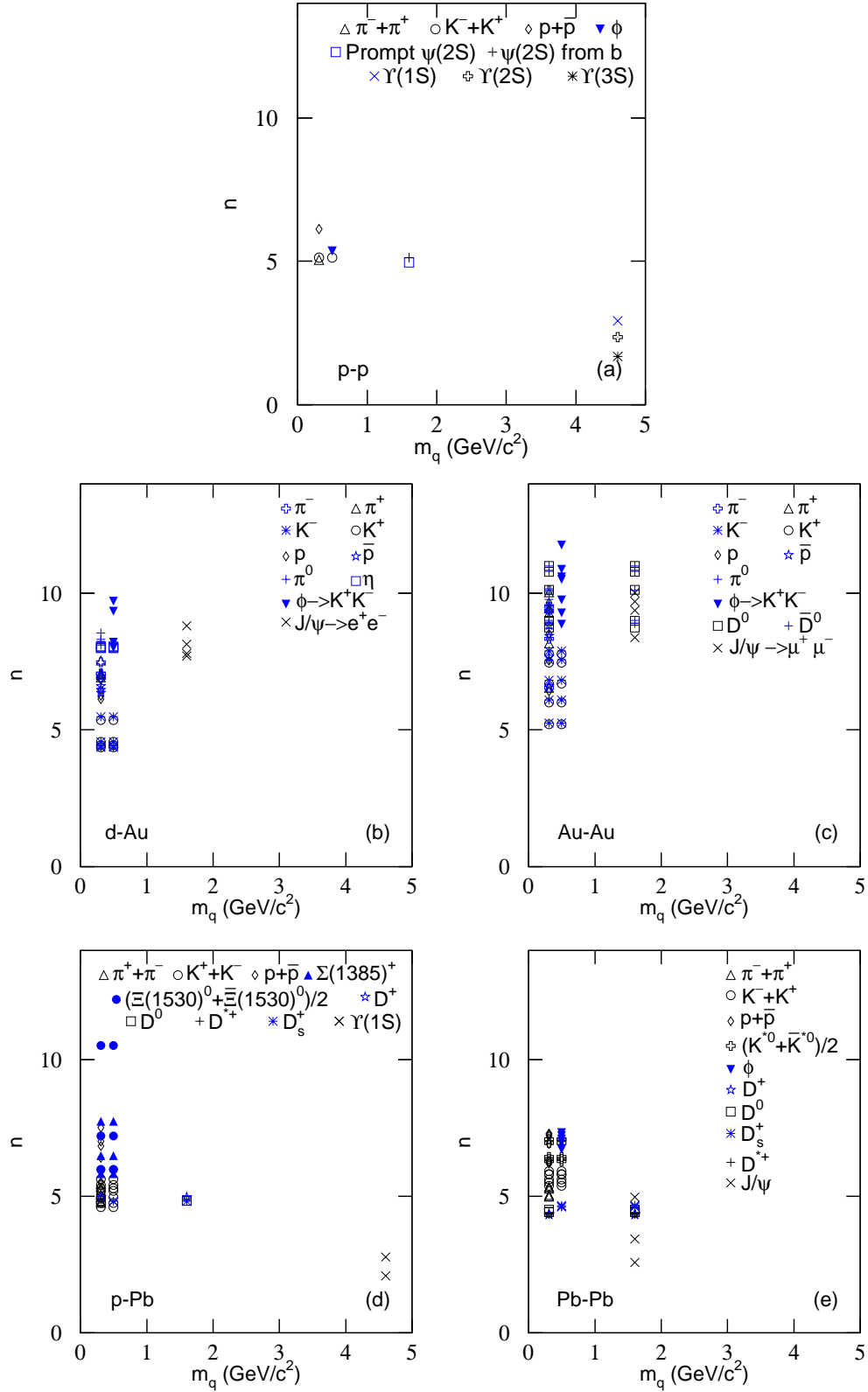


Figure 12: Dependence of parameter n on constituent mass m_q of quarks that make up hadrons produced in (a) p - p , (b) d -Au, (c) Au-Au, (d) p -Pb, and (e) Pb-Pb collisions at the RHIC or LHC. The obtained parameter values corresponding to various quarks are cited from Tables 1–5.

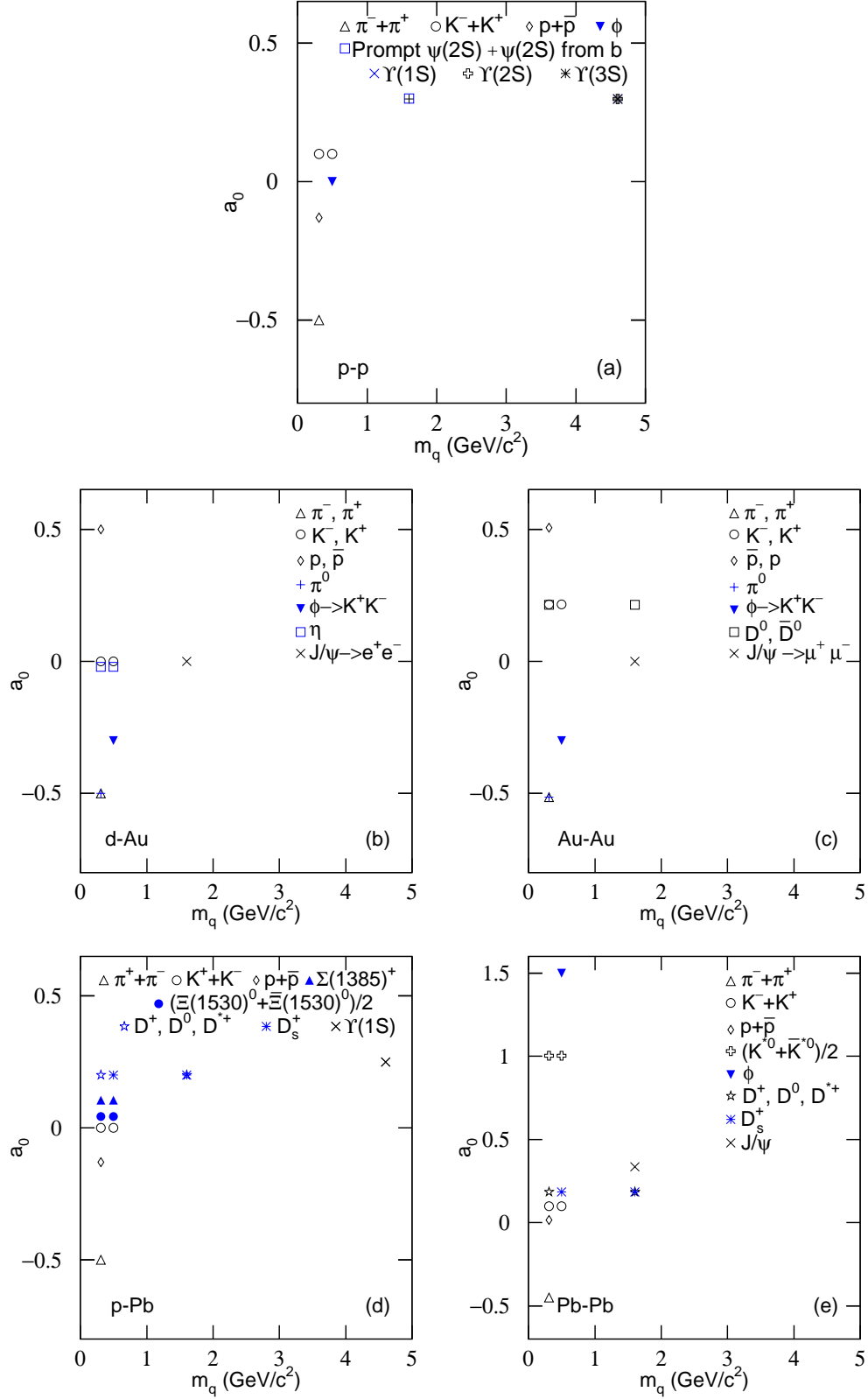


Figure 13: Dependence of parameter a_0 on constituent mass m_q of quarks that make up hadrons produced in (a) p - p , (b) d -Au, (c) Au-Au, (d) p -Pb, and (e) Pb-Pb collisions at the RHIC or LHC. The obtained parameter values corresponding to various quarks are cited from Tables 1–5.

collision system emits leptons [21], it also stays in an approximate equilibrium state. However, when the collision system emits jets [69], it stays in a non-equilibrium state in some cases. We may say that the concept of temperature is approximately applicable in most cases in high energy collisions.

In central collisions, we have obtained a larger T and n than those in peripheral collisions. This means that central collisions stay in higher excitation state and are closer to equilibrium state. This is caused by more energy deposition due to more participant nucleons in central collisions. For heavy hadrons and heavy flavor quarks, a larger T and smaller n are obtained due to early emission. In fact, in the early emission process, the collision system has higher temperature and has not enough time to reach to a closer equilibrium state. The early emission of heavy hadrons (and heavy flavor quarks) is a natural result of hydrodynamic behavior [86]. This is because that massive particles are left in the process of system evolution.

The revised index a_0 describes the winding degree of the spectra in very low transverse momentum region. Generally, $a_0 < 0$ is a reflection of increment in yield of light particles via resonance decay, while $a_0 > 0$ is a reflection of decrement in yield of heavy particles due to decay or absorption in hot and dense medium in participant region. In very low transverse momentum region, the present work shows that both the effects of the generation of light hadrons via resonance decay and the decay or absorption of heavy hadrons in hot and dense medium are obvious. The present work also shows that a_0 is independent of centrality. This reflects that the resonance generation and decay or absorption happen in the participant region, but not in the spectator region. We may neglect the cold (spectator) nuclear effect in the study of transverse momentum spectra.

Apart from in-medium effects which provide the environment of resonance and absorption, heavy ion collisions especially Pb-Pb collisions also have additional final state effects such as collective flow, recombination, and jet quenching in different p_T regions which finally contribute to the hadron spectra. These effects affect together the spectra in final state by increasing or decreasing p_T . In experiments, the contributions of these effects cannot be absolutely distinguished. We have uniformly described the different contributions by the convolution of TP-like functions. Apart from a_0 which determines the bending degree of curve in low p_T region and then affects the slope of curve in medium and high

p_T region, larger T or smaller n results in wider spectra, which decreases the probability in low p_T region and increases the probability in high p_T region.

Before summary and conclusions, we would like to point out that Eqs. (3) or (5) can fit meanwhile the spectra in low and medium-high transverse momentum regions which are contributed by the soft excitation and hard scattering processes respectively. For the spectra in low (or medium-high) transverse momentum region only, Eqs. (3) or (5) is expected to fit naturally. In low energy region such as in the RHIC Beam Energy Scan (BES) program or the Super Proton Synchrotron (SPS) and its BES program, the spectra are mainly contributed by the soft excitation process. The contribution fraction of the hard scattering process at low energy is less than that at the RHIC and LHC [23]. In particular, the contribution of hard process at low energy can be neglected in most cases.

Eqs. (3) or (5) can fit the spectra at the RHIC BES and the SPS authentically. In order to highlight the key points discussed above, we show the comparisons of Eqs. (3) or (5) with the experimental data measured at the SPS and RHIC BES in the Appendix A. As examples, only INEL p - p , central Au-Au, and central Pb-Pb collisions are included in Figs. 14–16, respectively.

4 Summary and conclusions

We summarize here our main observations and conclusions.

(a) We have studied the transverse momentum spectra of different hadrons produced in p - p , d -Au, Au-Au, p -Pb, and Pb-Pb collisions at different center-of-mass energies. The experimental data measured by the ALICE, CMS, LHCb, NA49, NA61/SHINE, PHENIX, and STAR Collaborations are collected and analyzed. In the framework of multisource thermal model at the quark level or the participant quark model, the fitting results are approximately in agreement with the experimental data.

(b) The TP-like function, i.e. the revised Tsallis-Pareto-type function, is used to describe the amount or portion contributed by each participant quark to the transverse momentum distribution of hadrons. The transverse momentum distribution of mesons is the convolution of two TP-like functions because the meson is composed of two quarks. The transverse momentum distribution of baryons is a convolution of three TP-like functions because the baryon is composed of three quarks. Not only for meson spectra but also for baryon spectra, the number of parameters is always four that includes three free parameters and a normalization constant. All free parameters are extracted at the quark level.

(c) For d -Au, Au-Au, p -Pb, and Pb-Pb collisions at high energies, in most cases, the effective temperature T and entropy index-related n extracted from the fits of transverse momentum spectra of hadrons increase with increasing the centrality from peripheral to central collisions. The revised index a_0 does not change with centrality. Peripheral collisions are further away from the equilibrium state, though the system in peripheral collisions is still close to the equilibrium state.

(d) The correlation trends of parameters T , n , and a_0 with the rest mass m_0 of hadron are in agreement with those of the mentioned parameters with the constituent mass m_q of quark, respectively. T has a positive correlation trend with mass. n has no obvious trend or has a negative correlation with mass. a_0 is positively related to mass. The production of hadrons with larger m_0 requires a higher T , and the corresponding state is further away from the equilibrium state, though the collision system is still close to the equilibrium state.

(e) High energy p - p and nuclear (p (d)- A or A - A) collisions show similar behaviors in many aspects, indicating that we may use the same function to fit uniformly the

spectra from both the collisions. These similarities exist commonly in high energy collisions from small system (p - p or p (d)- A) to large one (A - A), implying that the similar participant or contributor quarks take part in the production of given particles, in which the remaining spectator quarks do not affect mainly the particle spectrum.

Acknowledgments This work was supported by the National Natural Science Foundation of China under Grant Nos. 12047571, 11575103, and 11947418, the China Scholarship Council (Chinese Government Scholarship) under Grant No. 202008140170, the Shanxi Provincial Innovative Foundation for Graduate Education under Grant No. 2019SY053, the Scientific and Technological Innovation Programs of Higher Education Institutions in Shanxi (STIP) under Grant No. 201802017, the Shanxi Provincial Natural Science Foundation under Grant No. 201901D111043, and the Fund for Shanxi “1331 Project” Key Subjects Construction.

Data availability statement This manuscript has no associated data or the data will not be deposited. [Authors’ comment: The data used to support the findings of this study are included within the article and are cited at relevant places within the text as references.]

Compliance with ethical standards

Ethical approval The authors declare that they are in compliance with ethical standards regarding the content of this paper.

Disclosure The funding agencies have no role in the design of the study; in the collection, analysis, or interpretation of the data; in the writing of the manuscript, or in the decision to publish the results.

Conflict of interest The authors declare that there are no conflicts of interest regarding the publication of this paper.

Appendix A. Comparison with data at low energy

Figure 14 shows the transverse momentum spectra, $d^2N/dp_T dy$, of (a) π^+ and π^- , (b) K^+ and K^- , as well as (c) p and \bar{p} with $0 < y < 0.2$ produced in INEL p - p collisions at 6.3, 7.7, 8.8, 12.3, and 17.3 GeV. The

Table 2. Values of T , n , a_0 , N_0 , χ^2 , and ndof corresponding to the curves in Fig. 2. All the free parameters are extracted at the quark level.

Particle (quark structure)	Centrality (%)	T (GeV)	n	a_0	N_0	χ^2/ndof
π^- ($d\bar{u}$)	0 – 20	0.249 ± 0.001	7.466 ± 0.026	-0.500 ± 0.001	6.784 ± 0.029	47/20
	20 – 40	0.235 ± 0.001	7.066 ± 0.026	-0.500 ± 0.002	5.218 ± 0.028	34/20
	40 – 60	0.225 ± 0.001	6.924 ± 0.023	-0.500 ± 0.002	3.674 ± 0.011	54/20
	60 – 88	0.215 ± 0.001	7.064 ± 0.025	-0.500 ± 0.002	1.838 ± 0.011	81/20
	0 – 100	0.235 ± 0.001	7.154 ± 0.022	-0.500 ± 0.001	3.749 ± 0.016	64/20
π^+ ($u\bar{d}$)	0 – 20	0.249 ± 0.001	7.537 ± 0.022	-0.500 ± 0.002	6.881 ± 0.023	56/20
	20 – 40	0.235 ± 0.001	7.080 ± 0.023	-0.500 ± 0.001	5.276 ± 0.028	42/20
	40 – 60	0.225 ± 0.001	6.922 ± 0.023	-0.500 ± 0.002	3.720 ± 0.017	50/20
	60 – 88	0.215 ± 0.001	7.007 ± 0.022	-0.500 ± 0.002	1.850 ± 0.011	99/20
	0 – 100	0.235 ± 0.001	7.159 ± 0.015	-0.500 ± 0.001	3.790 ± 0.011	53/20
K^- ($s\bar{u}$)	0 – 20	0.186 ± 0.001	5.482 ± 0.018	0.000 ± 0.002	0.906 ± 0.007	80/17
	20 – 40	0.162 ± 0.001	4.560 ± 0.021	0.000 ± 0.005	0.677 ± 0.003	85/17
	40 – 60	0.153 ± 0.001	4.403 ± 0.020	0.000 ± 0.004	0.459 ± 0.003	70/17
	60 – 88	0.142 ± 0.001	4.365 ± 0.022	0.000 ± 0.003	0.225 ± 0.002	47/17
	0 – 100	0.169 ± 0.001	4.873 ± 0.021	0.000 ± 0.003	0.475 ± 0.002	129/17
K^+ ($u\bar{s}$)	0 – 20	0.186 ± 0.001	5.360 ± 0.024	0.000 ± 0.002	0.948 ± 0.013	89/17
	20 – 40	0.164 ± 0.001	4.562 ± 0.021	0.000 ± 0.002	0.706 ± 0.002	90/17
	40 – 60	0.156 ± 0.001	4.445 ± 0.022	0.000 ± 0.003	0.481 ± 0.003	39/17
	60 – 88	0.145 ± 0.001	4.360 ± 0.023	0.000 ± 0.003	0.233 ± 0.003	43/17
	0 – 100	0.172 ± 0.001	4.887 ± 0.019	0.000 ± 0.002	0.497 ± 0.002	110/17
\bar{p} ($\bar{u}\bar{u}\bar{d}$)	0 – 20	0.132 ± 0.001	6.955 ± 0.024	0.500 ± 0.001	0.013 ± 0.002	67/20
	20 – 40	0.125 ± 0.001	6.599 ± 0.023	0.500 ± 0.002	0.007 ± 0.000	47/20
	40 – 60	0.118 ± 0.001	6.461 ± 0.023	0.500 ± 0.002	0.003 ± 0.001	34/20
	60 – 88	0.109 ± 0.001	6.350 ± 0.024	0.500 ± 0.003	0.001 ± 0.000	42/20
	0 – 100	0.124 ± 0.001	6.622 ± 0.015	0.500 ± 0.002	0.003 ± 0.001	65/20
p (uud)	0 – 20	0.133 ± 0.001	6.831 ± 0.015	0.500 ± 0.002	0.023 ± 0.002	144/20
	20 – 40	0.125 ± 0.001	6.460 ± 0.019	0.500 ± 0.003	0.012 ± 0.001	100/20
	40 – 60	0.118 ± 0.001	6.252 ± 0.023	0.500 ± 0.003	0.005 ± 0.001	54/20
	60 – 88	0.109 ± 0.001	6.119 ± 0.023	0.500 ± 0.002	0.001 ± 0.001	76/20
	0 – 100	0.124 ± 0.001	6.441 ± 0.021	0.500 ± 0.003	0.006 ± 0.001	164/20
π^0 ($(u\bar{u} - d\bar{d})/\sqrt{2}$)	0 – 20	0.244 ± 0.001	8.539 ± 0.022	-0.500 ± 0.003	9.873 ± 0.072	4/17
	20 – 40	0.242 ± 0.001	8.312 ± 0.020	-0.500 ± 0.002	4.442 ± 0.036	11/17
	40 – 60	0.239 ± 0.001	8.236 ± 0.022	-0.500 ± 0.003	4.600 ± 0.036	10/17
	60 – 88	0.233 ± 0.001	8.109 ± 0.029	-0.500 ± 0.001	2.262 ± 0.021	6/17
	0 – 20	0.301 ± 0.002	9.704 ± 0.035	-0.300 ± 0.005	$(1.372 \pm 0.046) \times 10^{-1}$	6/6
ϕ ($s\bar{s}$)	20 – 40	0.298 ± 0.002	9.337 ± 0.032	-0.300 ± 0.003	$(9.028 \pm 0.072) \times 10^{-2}$	6/6
	40 – 60	0.288 ± 0.002	8.215 ± 0.034	-0.300 ± 0.005	$(4.816 \pm 0.108) \times 10^{-2}$	5/6
	60 – 88	0.254 ± 0.003	8.012 ± 0.037	-0.300 ± 0.003	$(3.248 \pm 0.056) \times 10^{-2}$	1/6
	0 – 20	0.212 ± 0.001	8.061 ± 0.025	-0.021 ± 0.002	0.527 ± 0.003	6/9
$\eta: \eta_q, \eta_s$ ($(u\bar{u} + d\bar{d})/\sqrt{2}, s\bar{s}$)	20 – 40	0.212 ± 0.001	8.023 ± 0.019	-0.021 ± 0.003	0.377 ± 0.003	5/9
	40 – 60	0.206 ± 0.001	8.001 ± 0.020	-0.021 ± 0.003	0.272 ± 0.003	3/9
	60 – 88	0.198 ± 0.001	7.992 ± 0.020	-0.021 ± 0.003	0.154 ± 0.001	8/8
	0 – 20	0.541 ± 0.002	11.391 ± 0.023	0.000 ± 0.004	$(8.807 \pm 0.088) \times 10^{-6}$	8/9
$J\psi \rightarrow e^+e^-$ ($c\bar{c}$)	20 – 40	0.525 ± 0.002	10.602 ± 0.030	0.000 ± 0.002	$(6.606 \pm 0.052) \times 10^{-6}$	10/9
	40 – 60	0.501 ± 0.001	10.352 ± 0.028	0.000 ± 0.002	$(4.404 \pm 0.013) \times 10^{-6}$	11/7
	60 – 88	0.481 ± 0.001	10.244 ± 0.022	0.000 ± 0.002	$(2.204 \pm 0.009) \times 10^{-6}$	4/7

Table 3. Values of T , n , a_0 , N_0 , χ^2 , and ndof corresponding to the curves in Fig. 3. All the free parameters are extracted at the quark level.

Particle (quark structure)	Centrality (%)	T (GeV)	n	a_0	N_0	χ^2/ndof
π^- ($d\bar{u}$)	0 – 10	0.237 ± 0.001	10.110 ± 0.023	-0.515 ± 0.002	300.364 ± 1.722	125/22
	10 – 20	0.236 ± 0.001	9.518 ± 0.021	-0.515 ± 0.002	205.734 ± 1.149	90/22
	20 – 40	0.240 ± 0.001	9.359 ± 0.033	-0.515 ± 0.001	109.609 ± 0.865	131/22
	40 – 60	0.231 ± 0.001	8.336 ± 0.024	-0.515 ± 0.002	20.677 ± 0.402	128/22
π^+ ($u\bar{d}$)	0 – 10	0.237 ± 0.001	10.040 ± 0.027	-0.515 ± 0.002	298.691 ± 1.723	168/22
	10 – 20	0.236 ± 0.001	9.457 ± 0.026	-0.515 ± 0.002	204.044 ± 0.977	109/22
	20 – 40	0.240 ± 0.001	9.288 ± 0.032	-0.515 ± 0.001	108.477 ± 0.577	166/22
	40 – 60	0.229 ± 0.001	8.159 ± 0.021	-0.515 ± 0.001	39.768 ± 0.386	116/22
K^- ($s\bar{u}$)	0 – 10	0.171 ± 0.001	7.887 ± 0.013	0.215 ± 0.002	39.205 ± 0.142	91/18
	10 – 20	0.171 ± 0.001	7.563 ± 0.022	0.215 ± 0.001	26.138 ± 0.085	65/18
	20 – 40	0.162 ± 0.001	6.814 ± 0.023	0.215 ± 0.002	14.428 ± 0.071	141/18
	40 – 60	0.151 ± 0.001	6.092 ± 0.018	0.215 ± 0.002	5.184 ± 0.028	123/18
K^+ ($u\bar{s}$)	0 – 10	0.171 ± 0.001	7.785 ± 0.022	0.215 ± 0.002	41.274 ± 0.214	49/18
	10 – 20	0.171 ± 0.001	7.453 ± 0.023	0.215 ± 0.002	27.651 ± 0.129	28/18
	20 – 40	0.162 ± 0.001	6.689 ± 0.021	0.215 ± 0.003	15.162 ± 0.021	55/18
	40 – 60	0.151 ± 0.001	6.005 ± 0.017	0.215 ± 0.002	5.480 ± 0.021	86/18
\bar{p} ($\bar{u}\bar{u}\bar{d}$)	0 – 10	0.157 ± 0.001	9.528 ± 0.017	0.505 ± 0.003	18.229 ± 0.091	181/22
	10 – 20	0.152 ± 0.001	8.828 ± 0.018	0.505 ± 0.004	8.639 ± 0.066	251/22
	20 – 40	0.148 ± 0.001	8.445 ± 0.016	0.505 ± 0.003	2.617 ± 0.024	281/22
	40 – 60	0.136 ± 0.001	7.677 ± 0.020	0.505 ± 0.002	0.372 ± 0.012	289/22
p (uud)	0 – 10	0.158 ± 0.001	9.651 ± 0.002	0.505 ± 0.003	33.974 ± 0.083	278/22
	10 – 20	0.158 ± 0.001	9.381 ± 0.013	0.505 ± 0.002	15.180 ± 0.091	157/22
	20 – 40	0.150 ± 0.000	8.520 ± 0.015	0.505 ± 0.004	4.617 ± 0.015	292/22
	40 – 60	0.136 ± 0.001	7.528 ± 0.019	0.505 ± 0.003	0.644 ± 0.008	254/22
π^0 ($(u\bar{u} - d\bar{d})/\sqrt{2}$)	0 – 10	0.246 ± 0.001	9.770 ± 0.026	-0.515 ± 0.003	254.832 ± 3.642	14/14
	10 – 20	0.246 ± 0.001	9.523 ± 0.027	-0.515 ± 0.003	195.664 ± 5.278	8/13
	20 – 30	0.246 ± 0.001	9.278 ± 0.022	-0.515 ± 0.002	134.019 ± 2.262	5/11
	30 – 40	0.246 ± 0.001	9.299 ± 0.020	-0.515 ± 0.002	94.639 ± 4.524	10/11
ϕ ($s\bar{s}$)	40 – 50	0.246 ± 0.001	8.940 ± 0.022	-0.515 ± 0.003	55.949 ± 0.377	3/10
	50 – 60	0.246 ± 0.001	8.909 ± 0.029	-0.515 ± 0.002	30.701 ± 0.226	2/10
	60 – 92	0.246 ± 0.001	8.710 ± 0.030	-0.515 ± 0.002	8.050 ± 0.150	3/10
	0 – 92	0.246 ± 0.001	9.133 ± 0.027	-0.515 ± 0.004	83.333 ± 2.262	19/18
D^0 ($c\bar{u}$)	0 – 10	0.290 ± 0.002	11.765 ± 0.034	-0.300 ± 0.003	9.694 ± 0.073	7/6
	10 – 20	0.290 ± 0.002	10.593 ± 0.035	-0.300 ± 0.003	6.954 ± 0.113	6/6
	20 – 30	0.290 ± 0.002	10.869 ± 0.040	-0.300 ± 0.004	4.832 ± 0.073	6/6
	30 – 40	0.290 ± 0.003	9.763 ± 0.031	-0.300 ± 0.003	3.072 ± 0.160	11/6
\bar{D}^0 ($u\bar{c}$)	40 – 50	0.290 ± 0.004	10.500 ± 0.030	-0.300 ± 0.003	1.996 ± 0.079	10/6
	50 – 60	0.265 ± 0.002	9.282 ± 0.026	-0.300 ± 0.005	1.271 ± 0.055	10/6
	60 – 92	0.271 ± 0.002	8.874 ± 0.024	-0.300 ± 0.004	0.257 ± 0.010	14/6
	0 – 92	0.291 ± 0.002	10.932 ± 0.025	-0.300 ± 0.003	3.041 ± 0.113	19/6
J/ψ ($c\bar{c}$)	0 – 10	0.295 ± 0.001	10.991 ± 0.026	0.214 ± 0.003	1.621 ± 0.012	3/7
	10 – 20	0.301 ± 0.001	10.786 ± 0.028	0.214 ± 0.003	1.005 ± 0.008	8/7
	20 – 40	0.307 ± 0.001	10.129 ± 0.021	0.214 ± 0.004	0.502 ± 0.003	11/7
	40 – 60	0.308 ± 0.001	8.746 ± 0.022	0.214 ± 0.002	0.150 ± 0.001	2/7
J/ψ ($c\bar{c}$)	60 – 80	0.308 ± 0.001	8.993 ± 0.025	0.214 ± 0.002	0.036 ± 0.001	5/6
	0 – 10	0.296 ± 0.001	10.999 ± 0.022	0.214 ± 0.003	1.696 ± 0.013	5/7
	10 – 20	0.303 ± 0.001	10.801 ± 0.021	0.214 ± 0.002	1.081 ± 0.010	4/7
	20 – 40	0.305 ± 0.001	10.104 ± 0.025	0.214 ± 0.003	0.553 ± 0.005	8/7
J/ψ ($c\bar{c}$)	40 – 60	0.308 ± 0.001	9.001 ± 0.020	0.214 ± 0.004	0.166 ± 0.001	4/6
	60 – 80	0.308 ± 0.001	8.892 ± 0.021	0.214 ± 0.003	0.034 ± 0.001	6/6
	0 – 20	0.455 ± 0.001	10.020 ± 0.001	0.000 ± 0.002	$(3.266 \pm 0.063) \times 10^{-4}$	5/5
	20 – 40	0.455 ± 0.002	9.689 ± 0.002	0.000 ± 0.002	$(1.633 \pm 0.031) \times 10^{-4}$	1/4
J/ψ ($c\bar{c}$)	40 – 60	0.450 ± 0.002	9.381 ± 0.002	0.000 ± 0.003	$(1.256 \pm 0.013) \times 10^{-4}$	5/4
	60 – 80	0.412 ± 0.003	8.375 ± 0.003	0.000 ± 0.002	$(1.633 \pm 0.003) \times 10^{-4}$	2/2
J/ψ ($c\bar{c}$)	0 – 80	0.449 ± 0.001	9.575 ± 0.001	0.000 ± 0.003	$(1.381 \pm 0.019) \times 10^{-4}$	1/5

symbols represent the experimental data measured by the NA61/SHINE Collaborations [87, 88] at the SPS. The curves are our fitted results by using Eqs. (3) for

mesons and (5) for baryons and the related parameters are listed in Table 6. One can see that the curves fit well the experimental data measured by the NA61/SHINE

Table 4. Values of T , n , a_0 , N_0 , χ^2 , and ndof corresponding to the curves in Fig. 4. All the free parameters are extracted at the quark level.

Particle (quark structure)	Centrality (%)	T (GeV)	n	a_0	N_0	χ^2/ndof
$\pi^+ + \pi^-$ ($u\bar{d}, d\bar{u}$)	0 – 5	0.305 ± 0.002	5.461 ± 0.020	-0.500 ± 0.002	21.932 ± 0.223	48/54
	5 – 10	0.300 ± 0.002	5.328 ± 0.022	-0.500 ± 0.004	20.741 ± 0.372	51/54
	10 – 20	0.294 ± 0.003	5.231 ± 0.023	-0.500 ± 0.004	14.987 ± 0.191	49/54
	20 – 40	0.281 ± 0.002	5.079 ± 0.031	-0.500 ± 0.005	11.566 ± 0.127	56/54
	40 – 60	0.266 ± 0.002	4.965 ± 0.021	-0.500 ± 0.004	8.129 ± 0.095	59/54
	60 – 80	0.244 ± 0.001	4.807 ± 0.023	-0.500 ± 0.001	5.055 ± 0.064	61/54
	80 – 100	0.210 ± 0.002	4.752 ± 0.010	-0.500 ± 0.003	2.239 ± 0.016	67/54
	NSD	0.279 ± 0.002	5.092 ± 0.022	-0.500 ± 0.004	8.509 ± 0.079	37/54
$K^+ + K^-$ ($u\bar{s}, s\bar{u}$)	0 – 5	0.267 ± 0.002	5.635 ± 0.023	0.000 ± 0.003	2.983 ± 0.223	20/47
	5 – 10	0.259 ± 0.001	5.421 ± 0.040	0.000 ± 0.004	2.375 ± 0.372	18/47
	10 – 20	0.251 ± 0.001	5.292 ± 0.022	0.000 ± 0.005	1.990 ± 0.013	11/47
	20 – 40	0.244 ± 0.002	5.201 ± 0.019	0.000 ± 0.004	1.511 ± 0.013	12/47
	40 – 60	0.225 ± 0.001	4.972 ± 0.018	0.000 ± 0.003	1.035 ± 0.013	18/47
	60 – 80	0.204 ± 0.002	4.752 ± 0.023	0.000 ± 0.002	0.616 ± 0.003	34/47
	80 – 100	0.171 ± 0.002	4.610 ± 0.010	0.000 ± 0.003	0.261 ± 0.003	47/47
	NSD	0.238 ± 0.001	5.158 ± 0.020	0.000 ± 0.003	1.121 ± 0.013	11/47
$p + \bar{p}$ ($uud, \bar{u}\bar{u}\bar{d}$)	0 – 5	0.334 ± 0.002	7.522 ± 0.029	-0.130 ± 0.002	1.801 ± 0.018	102/45
	5 – 10	0.319 ± 0.002	7.202 ± 0.024	-0.130 ± 0.002	1.521 ± 0.018	80/45
	10 – 20	0.311 ± 0.001	7.003 ± 0.031	-0.130 ± 0.002	1.325 ± 0.008	67/45
	20 – 40	0.298 ± 0.002	6.839 ± 0.021	-0.130 ± 0.002	1.051 ± 0.008	29/45
	40 – 60	0.269 ± 0.002	6.414 ± 0.038	-0.130 ± 0.002	0.814 ± 0.008	32/45
	60 – 80	0.237 ± 0.001	5.890 ± 0.031	-0.130 ± 0.004	0.553 ± 0.006	13/45
	80 – 100	0.195 ± 0.001	5.520 ± 0.025	-0.130 ± 0.004	0.269 ± 0.002	16/45
	NSD	0.292 ± 0.002	6.790 ± 0.021	-0.130 ± 0.003	0.801 ± 0.007	33/45
$\Sigma(1385)^+$ (uus)	0 – 20	0.336 ± 0.002	5.513 ± 0.037	-0.100 ± 0.003	$(0.048 \pm 0.226) \times 10^{-3}$	16/2
	20 – 60	0.299 ± 0.003	5.595 ± 0.040	-0.100 ± 0.004	$(0.028 \pm 0.570) \times 10^{-3}$	9/2
	60 – 100	0.281 ± 0.002	6.009 ± 0.050	-0.100 ± 0.004	$(0.007 \pm 0.115) \times 10^{-3}$	9/2
	NSD	0.329 ± 0.002	6.254 ± 0.032	-0.100 ± 0.002	$(0.024 \pm 0.567) \times 10^{-3}$	4/2
$(\Xi(1530)^0 + \bar{\Xi}(1530)^0)/2$ ($uss, \bar{u}\bar{s}\bar{s}$)	0 – 20	0.419 ± 0.003	9.896 ± 0.025	-0.100 ± 0.002	$(13.262 \pm 0.265) \times 10^{-3}$	5/6
	20 – 40	0.375 ± 0.002	8.553 ± 0.033	-0.100 ± 0.015	$(8.516 \pm 0.266) \times 10^{-3}$	1/6
	40 – 60	0.358 ± 0.002	7.195 ± 0.031	-0.100 ± 0.013	$(4.793 \pm 0.106) \times 10^{-3}$	4/6
	60 – 100	0.331 ± 0.002	7.637 ± 0.032	-0.100 ± 0.001	$(1.710 \pm 0.011) \times 10^{-3}$	2/6
NSD	0.377 ± 0.002	8.099 ± 0.041	-0.100 ± 0.002	$(5.905 \pm 0.005) \times 10^{-3}$	2/6	
$D^+ (c\bar{d})$	MB	0.445 ± 0.002	4.969 ± 0.021	0.200 ± 0.003	$(1.911 \pm 0.002) \times 10^{-2}$	4/14
$D^0 (c\bar{u})$	MB	0.439 ± 0.001	4.840 ± 0.022	0.200 ± 0.003	$(3.995 \pm 0.006) \times 10^{-2}$	4/15
$D^{*+} (c\bar{d})$	MB	0.470 ± 0.001	4.878 ± 0.021	0.200 ± 0.002	$(1.701 \pm 0.004) \times 10^{-2}$	2/13
$D_s^+ (c\bar{s})$	MB	0.421 ± 0.002	4.816 ± 0.024	0.200 ± 0.004	$(1.161 \pm 0.003) \times 10^{-2}$	2/1
$\Upsilon(1S) (b\bar{b}) (-4.46 < y < 2.96)$	MB	0.619 ± 0.004	2.778 ± 0.025	0.250 ± 0.003	$(2.719 \pm 0.075) \times 10^{-7}$	3/1
$\Upsilon(1S) (b\bar{b}) (2.03 < y < 3.53)$	MB	0.619 ± 0.002	2.098 ± 0.023	0.250 ± 0.002	$(4.522 \pm 0.090) \times 10^{-7}$	5/1

Collaboration.

Figure 15 shows the transverse momentum spectra, $(1/2\pi p_T)d^2N/dp_T dy$, of (a) π^+ and π^- , (b) K^+ and K^- , (c) p and \bar{p} , (d) K_S^0 , (e) Λ and $\bar{\Lambda}$, as well as (f) Ξ^+ and Ξ^- with (a)–(c) $|y| < 0.1$ and (d)–(f) $|y| < 0.5$ produced in 0–5% Au-Au collisions at 7.7, 11.5, 19.6, 27, and 39 GeV. The symbols represent the experimen-

tal data measured by the STAR Collaborations [89, 90] at the RHIC BES. The curves are our fitted results by using Eqs. (3) for mesons and (5) for baryons and the related parameters are listed in Table 7. One can see that the curves fit well the experimental data measured by the STAR Collaboration.

Table 5. Values of T , n , a_0 , N_0 , χ^2 , and ndof corresponding to the curves in Fig. 5, where “-” in the last column denotes ndof = 0 and the corresponding curve is for the eye guiding only. All the free parameters are extracted at the quark level.

Particle (quark structure)	Centrality (%)	T (GeV)	n	a_0	N_0	χ^2/ndof
$\pi^+ + \pi^-$ ($u\bar{d}, d\bar{u}$)	0 – 5	0.222 ± 0.001	5.343 ± 0.023	-0.450 ± 0.003	$(2.307 \pm 0.021) \times 10^3$	328/59
	5 – 10	0.220 ± 0.002	5.343 ± 0.022	-0.450 ± 0.002	$(2.013 \pm 0.012) \times 10^3$	255/59
	10 – 20	0.219 ± 0.001	5.285 ± 0.021	-0.450 ± 0.003	$(1.527 \pm 0.013) \times 10^3$	228/59
	20 – 40	0.215 ± 0.001	5.055 ± 0.023	-0.450 ± 0.003	$(8.979 \pm 0.085) \times 10^2$	162/59
	40 – 60	0.211 ± 0.001	5.005 ± 0.021	-0.450 ± 0.003	$(3.404 \pm 0.022) \times 10^2$	69/59
	60 – 80	0.207 ± 0.001	4.985 ± 0.020	-0.450 ± 0.004	$(9.571 \pm 0.075) \times 10^1$	20/59
$K^+ + K^-$ ($u\bar{s}, s\bar{u}$)	0 – 5	0.202 ± 0.001	5.923 ± 0.024	0.100 ± 0.004	$(3.451 \pm 0.033) \times 10^2$	434/54
	5 – 10	0.202 ± 0.002	5.822 ± 0.030	0.100 ± 0.002	$(2.682 \pm 0.022) \times 10^2$	751/54
	10 – 20	0.202 ± 0.002	5.802 ± 0.020	0.100 ± 0.003	$(2.225 \pm 0.022) \times 10^2$	309/54
	20 – 40	0.197 ± 0.001	5.608 ± 0.021	0.100 ± 0.004	$(1.271 \pm 0.011) \times 10^2$	208/54
	40 – 60	0.190 ± 0.001	5.505 ± 0.021	0.100 ± 0.004	$(4.964 \pm 0.045) \times 10^1$	55/54
	60 – 80	0.184 ± 0.001	5.385 ± 0.024	0.100 ± 0.004	$(1.279 \pm 0.011) \times 10^1$	26/54
$p + \bar{p}$ ($uud, \bar{u}\bar{u}\bar{d}$)	0 – 5	0.245 ± 0.002	7.296 ± 0.022	0.015 ± 0.003	$(1.083 \pm 0.012) \times 10^2$	631/45
	5 – 10	0.245 ± 0.001	7.266 ± 0.021	0.015 ± 0.003	$(9.408 \pm 0.015) \times 10^1$	519/45
	10 – 20	0.242 ± 0.002	7.216 ± 0.030	0.015 ± 0.003	$(7.186 \pm 0.115) \times 10^1$	485/45
	20 – 40	0.238 ± 0.002	6.916 ± 0.023	0.015 ± 0.004	$(3.946 \pm 0.035) \times 10^1$	345/45
	40 – 60	0.205 ± 0.002	6.276 ± 0.024	0.015 ± 0.002	$(1.734 \pm 0.012) \times 10^1$	234/45
	60 – 80	0.198 ± 0.002	6.200 ± 0.026	0.015 ± 0.004	4.955 ± 0.048	48/45
$(K^{*0} + \bar{K}^{*0})/2$ ($d\bar{s}, s\bar{d}$)	0 – 5	0.181 ± 0.002	7.088 ± 0.022	1.003 ± 0.003	19.493 ± 0.190	25/9
	5 – 10	0.180 ± 0.001	7.093 ± 0.024	1.003 ± 0.004	15.100 ± 0.317	22/9
	10 – 20	0.180 ± 0.002	6.952 ± 0.023	1.003 ± 0.005	12.930 ± 0.654	43/9
	20 – 30	0.169 ± 0.002	6.441 ± 0.024	1.003 ± 0.005	10.073 ± 0.095	24/9
	30 – 40	0.165 ± 0.002	6.361 ± 0.025	1.003 ± 0.004	7.144 ± 0.069	10/9
	40 – 50	0.163 ± 0.001	6.284 ± 0.024	1.003 ± 0.003	4.491 ± 0.019	6/9
ϕ ($s\bar{s}$)	0 – 5	0.135 ± 0.002	7.328 ± 0.016	1.500 ± 0.004	12.354 ± 0.089	37/13
	5 – 10	0.135 ± 0.001	7.222 ± 0.022	1.500 ± 0.005	10.560 ± 0.127	41/13
	10 – 20	0.135 ± 0.002	7.096 ± 0.024	1.500 ± 0.003	8.255 ± 0.065	33/13
	20 – 30	0.132 ± 0.001	7.002 ± 0.022	1.500 ± 0.004	6.401 ± 0.084	24/13
	30 – 40	0.129 ± 0.001	6.746 ± 0.020	1.500 ± 0.003	3.905 ± 0.072	14/13
	40 – 50	0.128 ± 0.001	6.717 ± 0.021	1.500 ± 0.003	2.497 ± 0.052	9/13
D^+ ($c\bar{d}$)	0 – 10	0.176 ± 0.001	4.352 ± 0.003	0.185 ± 0.001	12.217 ± 0.010	4/8
	30 – 50	0.230 ± 0.001	4.342 ± 0.006	0.185 ± 0.002	1.528 ± 0.010	6/7
	60 – 80	0.340 ± 0.002	4.329 ± 0.005	0.185 ± 0.002	0.079 ± 0.001	3/6
D^0 ($c\bar{u}$)	0 – 10	0.235 ± 0.001	4.505 ± 0.003	0.185 ± 0.002	12.364 ± 0.059	15/9
	30 – 50	0.297 ± 0.001	4.442 ± 0.002	0.185 ± 0.001	1.606 ± 0.007	3/8
	60 – 80	0.340 ± 0.001	4.421 ± 0.002	0.185 ± 0.002	0.166 ± 0.001	7/8
D^{*+} ($c\bar{d}$)	0 – 10	0.170 ± 0.001	4.396 ± 0.002	0.185 ± 0.003	16.500 ± 0.030	2/7
	30 – 50	0.297 ± 0.002	4.367 ± 0.005	0.185 ± 0.003	0.754 ± 0.003	4/7
	60 – 80	0.318 ± 0.001	4.346 ± 0.004	0.185 ± 0.002	0.108 ± 0.001	2/6
D_s^+ ($c\bar{s}$)	0 – 10	0.232 ± 0.001	4.670 ± 0.002	0.185 ± 0.001	6.074 ± 0.030	0.1/-
	30 – 50	0.291 ± 0.001	4.613 ± 0.005	0.185 ± 0.002	0.690 ± 0.003	0.4/-
	60 – 80	0.423 ± 0.001	4.613 ± 0.004	0.185 ± 0.002	0.043 ± 0.001	0.5/1
J/ψ ($c\bar{c}$)	0 – 20	0.382 ± 0.001	4.975 ± 0.004	0.335 ± 0.001	$(19.036 \pm 0.179) \times 10^{-2}$	0.5/-
	20 – 40	0.338 ± 0.001	3.445 ± 0.005	0.335 ± 0.002	$(5.692 \pm 0.044) \times 10^{-2}$	1/-
	40 – 90	0.269 ± 0.001	2.575 ± 0.005	0.335 ± 0.002	$(0.761 \pm 0.058) \times 10^{-2}$	9/-

The transverse mass ($m_T = \sqrt{p_T^2 + m_0^2}$) (minus rest mass m_0) spectra, $(1/m_T)d^2N/dm_T dy$, of (a) π^+ and π^- , (b) K^+ and K^- , (c) p and \bar{p} , (d) ϕ , (e) Λ and $\bar{\Lambda}$, as well as (f) Ξ^+ and Ξ^- with (a)–(c), (e), and (f)

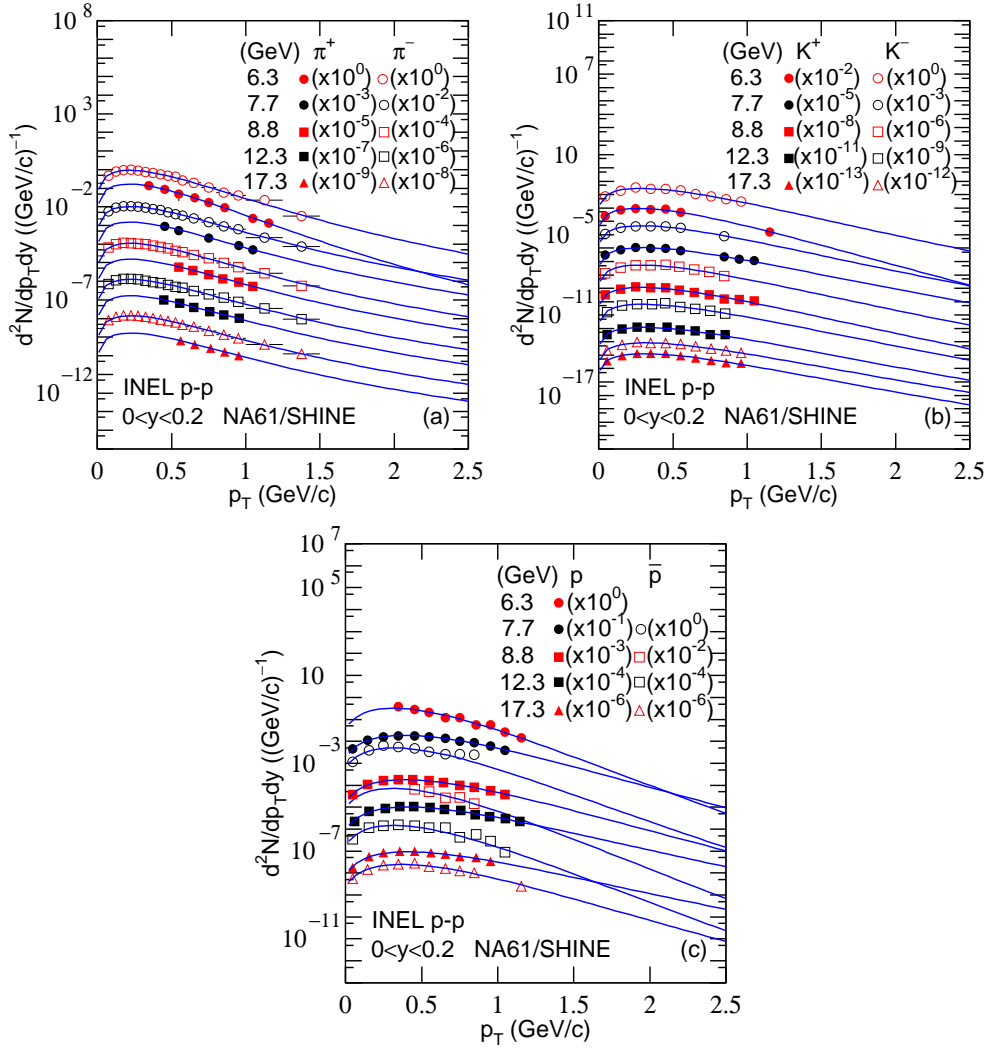


Figure 14: The transverse momentum spectra of (a) π^+ and π^- , (b) K^+ and K^- , as well as (c) p and \bar{p} with $0 < y < 0.2$ produced in INEL p - p collisions at 6.3, 7.7, 8.8, 12.3, and 17.3 GeV. The symbols represent the experimental data measured by the NA61/SHINE Collaborations [87, 88] at the SPS and the curves are our fitted results by using Eqs. (3) for mesons and (5) for baryons.

$0 < y < 0.2$, as well as (d) $0 < y < 1.0$ to $0 < y < 1.8$ produced in central (0–5% to 0–10%) Pb-Pb collisions at 6.3, 7.6, 8.8, 12.3, and 17.3 GeV are shown in Fig. 16. The symbols represent the experimental data measured by the NA49 Collaborations [91, 92, 93, 94, 95] at the SPS and the curves are our fitted results by using Eqs. (3) for mesons and (5) for baryons. The related parameters are listed in Table 8 and the curves fit well the experimental data measured by the NA49 Collaboration.

Comparing with high energy collisions, low energy collisions show low effective temperature T . Over an energy range decreasing from the LHC to SPS or RHIC

BES, the entropy index-related n increases and the revised index a_0 do not show significant variation. The conclusions obtained from high energy collisions are coordinated with those from low energy collisions, though the energy dependent T and n are observed. It is natural that low energy collisions result in low effective temperature due to low energy deposition during the collision process. At low energy, the long collision time renders closer to equilibrium, in which n is large and q is small.

The collisions at SPS or RHIC BES provide an opportunity to study the dependence of T and n on $\sqrt{s_{NN}}$ around the critical point/region of the deconfinement phase transition from hadronic matter to QGP. Our ex-

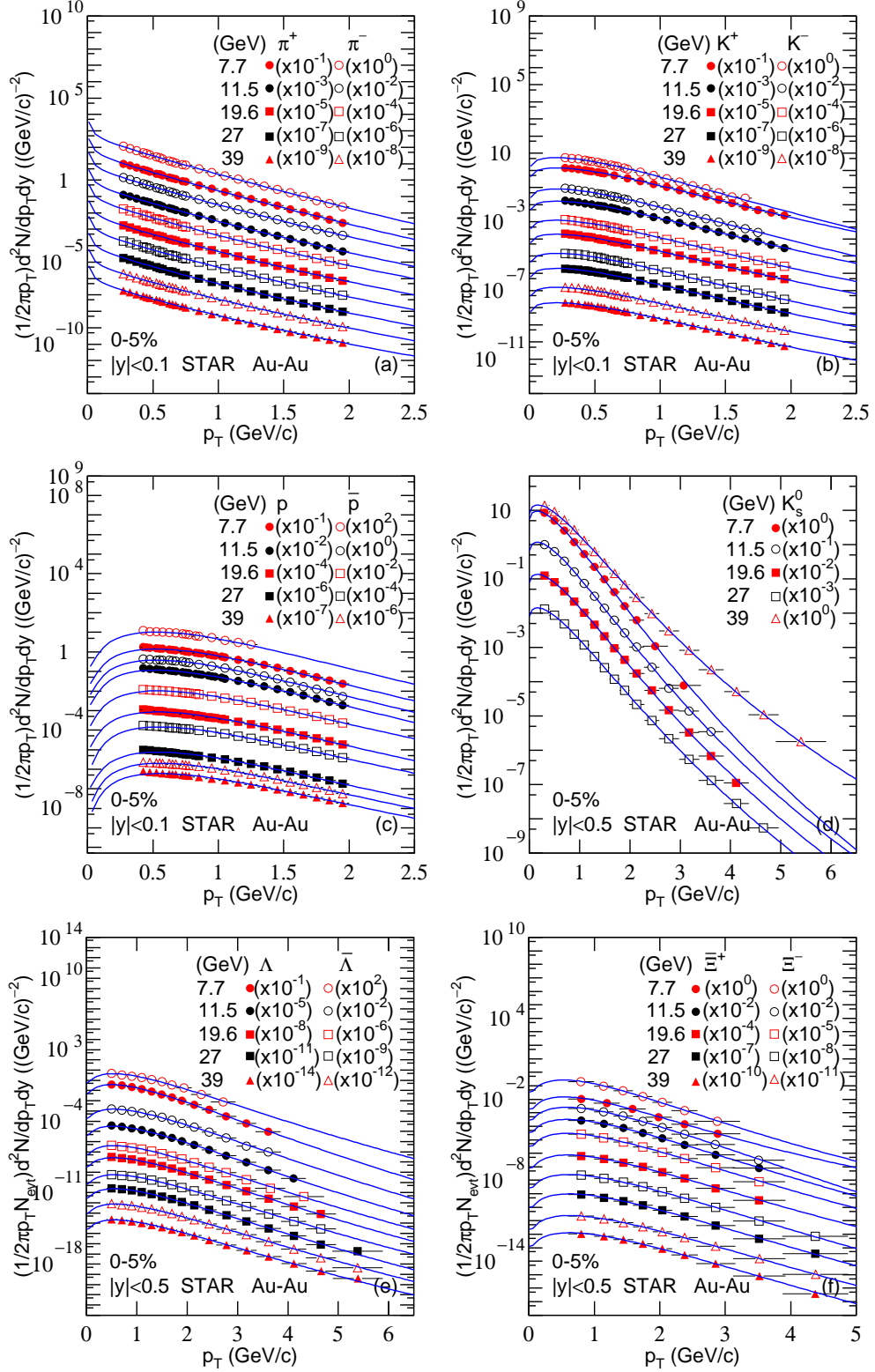


Figure 15: The transverse momentum spectra of (a) π^+ and π^- , (b) K^+ and K^- , (c) p and \bar{p} , (d) K_S^0 , (e) Λ and $\bar{\Lambda}$, as well as (f) Ξ^+ and Ξ^- with (a)–(c) $|y| < 0.1$ and (d)–(f) $|y| < 0.5$ produced in 0–5% Au–Au collisions at 7.7, 11.5, 19.6, 27, and 39 GeV. The symbols represent the experimental data measured by the STAR Collaborations [89, 90] at the RHIC BES and the curves are our fitted results by using Eqs. (3) for mesons and (5) for baryons.

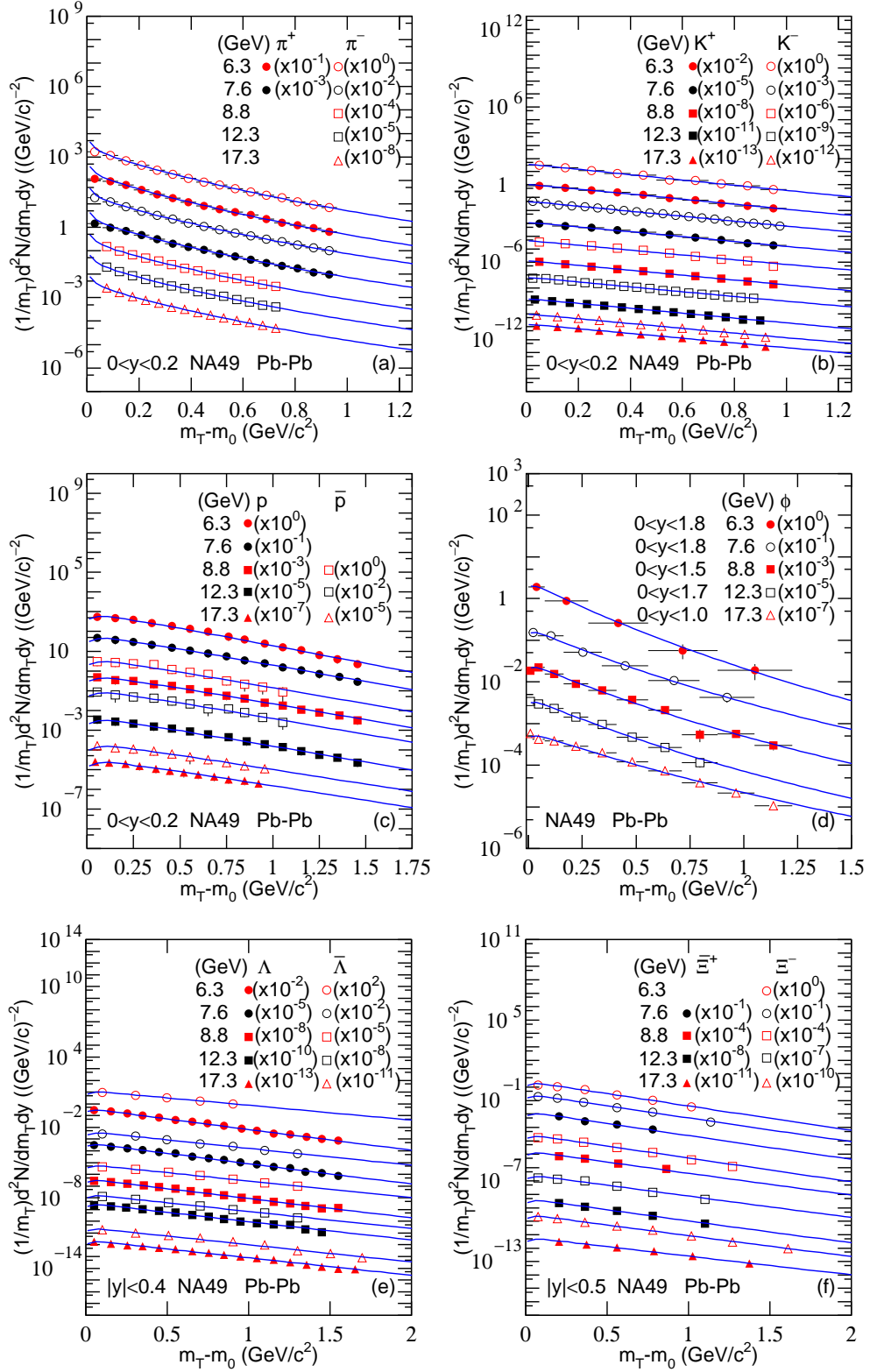


Figure 16: The transverse mass spectra of (a) π^+ and π^- , (b) K^+ and K^- , (c) p and \bar{p} , (d) ϕ , (e) Λ and $\bar{\Lambda}$, as well as (f) Ξ^+ and Ξ^- with (a)–(c), (e), and (f) $0 < y < 0.2$, as well as (d) $0 < y < 1.0$ to $0 < y < 1.8$ produced in central (0–5% to 0–10%) Pb-Pb collisions at 6.3, 7.6, 8.8, 12.3, and 17.3 GeV. The symbols represent the experimental data measured by the NA49 Collaborations [91, 92, 93, 94, 95] at the SPS and the curves are our fitted results by using Eqs. (3) for mesons and (5) for baryons.

Table 6. Values of T , n , a_0 , N_0 , χ^2 , and ndof corresponding to the curves in Fig. 14. All the free parameters are extracted at the quark level.

Particle (quark structure)	Energy (GeV)	T (GeV)	n	a_0	N_0	χ^2/ndof
π^- ($d\bar{u}$)	6.3	0.090 ± 0.001	9.965 ± 0.040	-0.03 ± 0.003	0.082 ± 0.001	7/14
	7.7	0.092 ± 0.001	7.847 ± 0.041	-0.03 ± 0.001	0.095 ± 0.001	14/14
	8.8	0.092 ± 0.001	7.857 ± 0.043	-0.03 ± 0.002	0.102 ± 0.001	24/14
	12.3	0.092 ± 0.001	7.212 ± 0.048	-0.03 ± 0.002	0.120 ± 0.001	23/14
	17.3	0.093 ± 0.001	6.978 ± 0.052	-0.03 ± 0.001	0.134 ± 0.002	13/14
π^+ ($u\bar{d}$)	6.3	0.090 ± 0.001	15.667 ± 0.037	-0.03 ± 0.002	0.014 ± 0.001	0.1/3
	7.7	0.091 ± 0.001	7.602 ± 0.036	-0.03 ± 0.002	0.142 ± 0.001	0.3/1
	8.8	0.092 ± 0.001	7.444 ± 0.035	-0.03 ± 0.003	0.145 ± 0.001	0.1/2
	12.3	0.092 ± 0.001	6.949 ± 0.051	-0.03 ± 0.002	0.160 ± 0.001	0.2/2
	17.3	0.093 ± 0.001	6.908 ± 0.034	-0.03 ± 0.001	0.160 ± 0.001	0.1/1
K^- ($s\bar{u}$)	6.3	0.113 ± 0.001	23.368 ± 0.053	0.000 ± 0.002	$(3.207 \pm 0.002) \times 10^{-3}$	3/6
	7.7	0.115 ± 0.001	21.249 ± 0.045	0.000 ± 0.002	$(5.212 \pm 0.020) \times 10^{-3}$	1/3
	8.8	0.116 ± 0.001	21.921 ± 0.043	0.000 ± 0.002	$(6.014 \pm 0.004) \times 10^{-3}$	2/5
	12.3	0.125 ± 0.002	21.703 ± 0.054	0.000 ± 0.002	$(7.417 \pm 0.023) \times 10^{-3}$	2/5
	17.3	0.136 ± 0.001	18.997 ± 0.052	0.000 ± 0.001	$(1.042 \pm 0.008) \times 10^{-2}$	1/6
K^+ ($u\bar{s}$)	6.3	0.103 ± 0.001	42.776 ± 0.053	0.000 ± 0.002	$(9.224 \pm 0.006) \times 10^{-3}$	1/3
	7.7	0.124 ± 0.002	20.001 ± 0.051	0.000 ± 0.002	$(1.262 \pm 0.020) \times 10^{-2}$	1/5
	8.8	0.117 ± 0.001	24.979 ± 0.052	0.000 ± 0.001	$(1.283 \pm 0.001) \times 10^{-2}$	4/7
	12.3	0.129 ± 0.001	20.018 ± 0.051	0.000 ± 0.002	$(1.443 \pm 0.012) \times 10^{-2}$	2/5
	17.3	0.132 ± 0.001	19.081 ± 0.064	0.000 ± 0.001	$(1.563 \pm 0.013) \times 10^{-2}$	1/6
\bar{p} ($\bar{u}\bar{u}\bar{d}$)	7.7	0.103 ± 0.001	19.411 ± 0.051	-0.09 ± 0.001	$(5.909 \pm 0.029) \times 10^{-4}$	12/5
	8.8	0.101 ± 0.001	28.003 ± 0.061	-0.09 ± 0.003	$(8.208 \pm 0.059) \times 10^{-4}$	5/1
	12.3	0.104 ± 0.002	25.826 ± 0.043	-0.09 ± 0.002	$(1.714 \pm 0.014) \times 10^{-3}$	15/7
	17.3	0.128 ± 0.001	17.847 ± 0.054	-0.09 ± 0.002	$(3.401 \pm 0.028) \times 10^{-3}$	1/16
p (uud)	6.3	0.103 ± 0.001	24.299 ± 0.057	-0.09 ± 0.002	$(3.279 \pm 0.029) \times 10^{-2}$	4/5
	7.7	0.138 ± 0.001	19.765 ± 0.056	-0.09 ± 0.002	$(2.715 \pm 0.022) \times 10^{-2}$	0.5/7
	8.8	0.139 ± 0.001	18.627 ± 0.044	-0.09 ± 0.001	$(2.570 \pm 0.022) \times 10^{-2}$	1/7
	12.3	0.147 ± 0.001	12.403 ± 0.051	-0.09 ± 0.001	$(1.583 \pm 0.013) \times 10^{-2}$	2/8
	17.3	0.147 ± 0.001	11.023 ± 0.044	-0.09 ± 0.001	$(1.460 \pm 0.014) \times 10^{-2}$	1/6

ploratory test shows that two parameterized functions are needed for the relation of T versus $\sqrt{s_{\text{NN}}}$. In the region of $\sqrt{s_{\text{NN}}} < 8$ GeV, $T = a_1[1 - \exp(-\sqrt{s_{\text{NN}}}/b_1)]$. In the region of $\sqrt{s_{\text{NN}}} \geq 8$ GeV, $T = a_2 \ln(\sqrt{s_{\text{NN}}}) + b_2$. Here, T , $\sqrt{s_{\text{NN}}}$, and four parameters ($a_{1,2}$ and $b_{1,2}$) are in the units of GeV. The parameters are particle dependent due to individual fitting. We have not used the simultaneous fitting in the present work due to unsatisfactory results.

Meanwhile, single parameterized function, $n = a_3 \exp(-\sqrt{s_{\text{NN}}}/b_3) + c_3$, is needed for the relation of n versus $\sqrt{s_{\text{NN}}}$, where the parameters are particle dependent, a_3 and c_3 are dimensionless, and b_3 is in the units of GeV. The increase of n means the decrease of q at lower energy, where the system is closer to the equilibrium due to enough and longer interaction time.

Because very limited collision systems at given energy are studied, the parameterized functions of T and n versus system size are not available here. Generally, with the increase of system size, T and n increase slightly or do not show significant change. For large system, more energies were deposited and more multiple scatterings had happened in the collisions, which cases T and n to have tendency of slight increase.

References

- [1] BRAHMS Collaboration (I. Arsene *et al.*), Nucl. Phys. A **757**, 1 (2005)
- [2] PHENIX Collaboration (K. Adcox *et al.*), Nucl. Phys. A **757**, 184 (2005)

Table 7. Values of T , n , a_0 , N_0 , χ^2 , and ndof corresponding to the curves in Fig. 15. All the free parameters are extracted at the quark level.

Particle (quark structure)	Energy (GeV)	T (GeV)	n	a_0	N_0	χ^2 /ndof
π^- ($d\bar{u}$)	7.7	0.198 ± 0.001	31.328 ± 0.053	-0.461 ± 0.002	24.185 ± 0.052	8/22
	11.5	0.197 ± 0.001	18.782 ± 0.051	-0.461 ± 0.002	31.347 ± 0.078	3/22
	19.6	0.202 ± 0.001	15.002 ± 0.053	-0.461 ± 0.002	39.916 ± 0.052	2/22
	27	0.208 ± 0.001	15.368 ± 0.054	-0.461 ± 0.001	43.343 ± 0.262	4/22
	39	0.216 ± 0.001	14.765 ± 0.052	-0.461 ± 0.001	44.444 ± 0.262	1/22
π^+ ($u\bar{d}$)	7.7	0.199 ± 0.001	27.972 ± 0.047	-0.461 ± 0.001	23.299 ± 0.131	8/22
	11.5	0.201 ± 0.001	18.362 ± 0.053	-0.461 ± 0.001	29.938 ± 0.131	2/22
	19.6	0.204 ± 0.001	15.042 ± 0.052	-0.461 ± 0.001	39.131 ± 0.078	1/22
	27	0.209 ± 0.001	14.512 ± 0.061	-0.461 ± 0.002	42.245 ± 0.262	2/22
	39	0.218 ± 0.001	13.912 ± 0.064	-0.461 ± 0.001	43.643 ± 0.104	0.4/22
K^- ($s\bar{u}$)	7.7	0.139 ± 0.001	18.572 ± 0.053	0.215 ± 0.003	1.441 ± 0.005	9/19
	11.5	0.145 ± 0.001	16.550 ± 0.054	0.215 ± 0.001	2.307 ± 0.011	6/19
	19.6	0.144 ± 0.001	11.102 ± 0.063	0.215 ± 0.002	3.573 ± 0.016	11/22
	27	0.149 ± 0.001	12.572 ± 0.054	0.215 ± 0.003	4.314 ± 0.018	7/21
	39	0.153 ± 0.001	10.179 ± 0.052	0.215 ± 0.001	4.776 ± 0.031	6/22
K^+ ($u\bar{s}$)	7.7	0.145 ± 0.001	13.392 ± 0.057	0.215 ± 0.002	3.974 ± 0.021	3/19
	11.5	0.149 ± 0.001	13.199 ± 0.056	0.215 ± 0.002	4.752 ± 0.022	6/21
	19.6	0.147 ± 0.001	10.660 ± 0.062	0.215 ± 0.002	5.629 ± 0.031	9/22
	27	0.152 ± 0.001	10.892 ± 0.051	0.215 ± 0.002	5.942 ± 0.031	1/22
	39	0.156 ± 0.001	11.100 ± 0.064	0.215 ± 0.001	6.105 ± 0.037	4/22
\bar{p} ($\bar{u}\bar{u}\bar{d}$)	7.7	0.141 ± 0.001	13.393 ± 0.063	0.325 ± 0.002	0.070 ± 0.001	7/11
	11.5	0.141 ± 0.001	13.374 ± 0.058	0.325 ± 0.002	0.260 ± 0.002	9/19
	19.6	0.147 ± 0.001	11.929 ± 0.063	0.325 ± 0.002	0.754 ± 0.006	11/18
	27	0.149 ± 0.002	11.328 ± 0.064	0.325 ± 0.003	1.101 ± 0.007	15/18
	39	0.151 ± 0.002	11.028 ± 0.052	0.325 ± 0.001	1.553 ± 0.012	10/19
p (uud)	7.7	0.142 ± 0.001	13.328 ± 0.057	0.325 ± 0.003	9.542 ± 0.093	18/25
	11.5	0.141 ± 0.001	13.328 ± 0.066	0.325 ± 0.003	7.838 ± 0.066	14/24
	19.6	0.145 ± 0.001	11.919 ± 0.062	0.325 ± 0.002	6.101 ± 0.039	27/25
	27	0.147 ± 0.002	11.336 ± 0.064	0.325 ± 0.001	5.506 ± 0.041	19/19
	39	0.151 ± 0.001	10.705 ± 0.064	0.325 ± 0.003	4.706 ± 0.038	17/18
K_S^0 ($d\bar{s}$)	7.7	0.168 ± 0.001	24.852 ± 0.055	0.111 ± 0.002	12.225 ± 0.068	9/8
	11.5	0.171 ± 0.001	20.572 ± 0.056	0.111 ± 0.002	15.673 ± 0.075	12/10
	19.6	0.183 ± 0.001	21.191 ± 0.062	0.111 ± 0.001	20.065 ± 0.112	6/11
	27	0.189 ± 0.001	19.796 ± 0.051	0.111 ± 0.001	22.010 ± 0.075	12/12
	39	0.194 ± 0.001	17.522 ± 0.054	0.111 ± 0.001	22.889 ± 0.125	6/13
$\bar{\Lambda}$ ($\bar{u}\bar{d}\bar{s}$)	7.7	0.187 ± 0.001	30.125 ± 0.063	0.171 ± 0.002	0.187 ± 0.001	9/6
	11.5	0.190 ± 0.001	41.964 ± 0.066	0.171 ± 0.002	0.626 ± 0.004	12/9
	19.6	0.195 ± 0.002	33.201 ± 0.062	0.171 ± 0.002	1.742 ± 0.006	29/10
	27	0.201 ± 0.001	30.202 ± 0.064	0.171 ± 0.002	2.598 ± 0.019	18/11
	39	0.205 ± 0.001	29.339 ± 0.058	0.171 ± 0.002	3.609 ± 0.025	8/12
Λ (uds)	7.7	0.175 ± 0.001	37.155 ± 0.067	0.171 ± 0.002	13.904 ± 0.064	4/9
	11.5	0.183 ± 0.001	34.466 ± 0.066	0.171 ± 0.002	12.856 ± 0.064	8/10
	19.6	0.194 ± 0.001	32.856 ± 0.062	0.171 ± 0.002	11.357 ± 0.070	13/11
	27	0.198 ± 0.001	30.723 ± 0.051	0.171 ± 0.003	10.706 ± 0.060	19/12
	39	0.204 ± 0.001	25.445 ± 0.054	0.171 ± 0.003	2.616 ± 0.058	17/12
Ξ^+ (dss)	7.7	0.162 ± 0.001	11.968 ± 0.063	0.195 ± 0.002	0.064 ± 0.004	2/2
	11.5	0.188 ± 0.001	23.869 ± 0.064	0.195 ± 0.003	0.154 ± 0.001	2/4
	19.6	0.196 ± 0.001	21.459 ± 0.053	0.195 ± 0.003	0.385 ± 0.003	11/7
	27	0.207 ± 0.001	28.733 ± 0.054	0.195 ± 0.002	0.533 ± 0.003	8/5
	39	0.210 ± 0.001	29.019 ± 0.062	0.195 ± 0.002	0.712 ± 0.006	3/5
Ξ^- (dss)	7.7	0.158 ± 0.001	16.351 ± 0.057	0.195 ± 0.002	1.071 ± 0.009	4/3
	11.5	0.187 ± 0.001	38.872 ± 0.055	0.195 ± 0.002	1.177 ± 0.012	2/4
	19.6	0.187 ± 0.001	21.236 ± 0.062	0.195 ± 0.001	1.428 ± 0.014	3/4
	27	0.201 ± 0.001	28.249 ± 0.061	0.195 ± 0.001	1.388 ± 0.019	4/5
	39	0.211 ± 0.001	27.631 ± 0.064	0.195 ± 0.002	1.354 ± 0.012	0.3/5

- [3] STAR Collaboration (J. Adams *et al.*), Nucl. Phys. A **757**, 102 (2005)
- [4] ALICE Collaboration (J. Schukraft *et al.*), Phil. Trans. Roy. Soc. Lond. A **370**, 917 (2012)
- [5] E.K.G. Sarkisyan, A.S. Sakharov, AIP Conf. Proc. **828**, 35 (2006)
- [6] E.K.G. Sarkisyan, A.S. Sakharov, Eur. Phys. J. C **70**, 533 (2010)
- [7] A.N. Mishra, R. Sahoo, E.K.G. Sarkisyan, A.S. Sakharov, Eur. Phys. J. C **74**, 3147 (2014)
- [8] E.K.G. Sarkisyan, A.N. Mishra, R. Sahoo, A.S. Sakharov, Phys. Rev. D **93**, 054046 (2016)
- [9] E.K.G. Sarkisyan, A.N. Mishra, R. Sahoo, A.S. Sakharov, Phys. Rev. D **94**, 011501 (2016)
- [10] E.K.G. Sarkisyan, A.N. Mishra, R. Sahoo, A.S. Sakharov, EPL **127**, 62001 (2019)

Table 8. Values of T , n , a_0 , N_0 , χ^2 , and ndof corresponding to the curves in Fig. 16, where “-” in the last column denotes ndof = 0 and the corresponding curve is for the eye guiding only. All the free parameters are extracted at the quark level.

Particle (quark structure)	Energy (GeV)	T (GeV)	n	a_0	N_0	χ^2 /ndof
π^- ($d\bar{u}$)	6.3	0.132 ± 0.001	4.851 ± 0.033	-0.460 ± 0.002	14.849 ± 0.043	34/12
	7.6	0.148 ± 0.001	4.771 ± 0.035	-0.460 ± 0.001	17.169 ± 0.044	28/12
	8.8	0.151 ± 0.001	4.771 ± 0.036	-0.460 ± 0.002	18.662 ± 0.074	38/10
	12.3	0.151 ± 0.001	4.706 ± 0.040	-0.460 ± 0.002	24.540 ± 0.077	16/10
	17.3	0.152 ± 0.001	4.427 ± 0.036	-0.460 ± 0.001	31.147 ± 0.053	17/10
π^+ ($u\bar{d}$)	6.3	0.139 ± 0.001	5.348 ± 0.030	-0.460 ± 0.002	13.773 ± 0.058	47/12
	7.6	0.152 ± 0.001	4.891 ± 0.031	-0.460 ± 0.001	16.212 ± 0.059	34/12
K^- ($s\bar{u}$)	6.3	0.160 ± 0.002	14.142 ± 0.043	0.030 ± 0.003	0.742 ± 0.004	20/6
	7.6	0.169 ± 0.001	12.962 ± 0.041	0.030 ± 0.001	1.087 ± 0.006	62/16
	8.8	0.176 ± 0.002	12.962 ± 0.038	0.030 ± 0.002	1.075 ± 0.010	55/6
	12.3	0.176 ± 0.001	12.962 ± 0.039	0.030 ± 0.003	1.542 ± 0.014	65/14
	17.3	0.178 ± 0.001	12.999 ± 0.032	0.030 ± 0.002	2.258 ± 0.009	33/8
K^+ ($u\bar{s}$)	6.3	0.177 ± 0.001	19.962 ± 0.032	0.030 ± 0.003	2.270 ± 0.013	33/6
	7.6	0.182 ± 0.001	19.002 ± 0.038	0.030 ± 0.002	2.780 ± 0.008	90/6
	8.8	0.182 ± 0.001	19.002 ± 0.042	0.030 ± 0.001	2.956 ± 0.013	39/6
	12.3	0.182 ± 0.001	18.992 ± 0.041	0.030 ± 0.003	3.390 ± 0.007	13/10
	17.3	0.187 ± 0.001	18.599 ± 0.044	0.030 ± 0.002	3.822 ± 0.027	40/8
\bar{p} ($\bar{u}\bar{u}\bar{d}$)	8.8	0.220 ± 0.002	50.042 ± 0.053	0.000 ± 0.003	0.095 ± 0.002	2/7
	12.3	0.222 ± 0.002	48.023 ± 0.051	0.000 ± 0.003	0.255 ± 0.003	1/7
	17.3	0.238 ± 0.001	40.923 ± 0.053	0.000 ± 0.002	0.562 ± 0.007	0.3/6
p (uud)	6.3	0.202 ± 0.001	55.040 ± 0.045	0.000 ± 0.002	16.158 ± 0.218	3/11
	7.6	0.216 ± 0.002	53.015 ± 0.046	0.000 ± 0.002	13.813 ± 0.223	1/11
	8.8	0.222 ± 0.002	53.015 ± 0.052	0.000 ± 0.002	14.234 ± 0.225	2/11
	12.3	0.222 ± 0.001	53.013 ± 0.055	0.000 ± 0.002	10.167 ± 0.225	2/11
	17.3	0.238 ± 0.001	43.969 ± 0.054	0.000 ± 0.001	8.582 ± 0.061	1/8
ϕ ($s\bar{s}$)	6.3	0.157 ± 0.001	7.992 ± 0.046	0.150 ± 0.001	0.504 ± 0.004	0.4/1
	7.6	0.179 ± 0.001	6.592 ± 0.044	0.150 ± 0.001	0.504 ± 0.003	1/2
	8.8	0.181 ± 0.001	6.592 ± 0.042	0.150 ± 0.001	0.620 ± 0.007	11/6
	12.3	0.181 ± 0.001	6.592 ± 0.041	0.150 ± 0.002	1.023 ± 0.004	6/4
	17.3	0.222 ± 0.002	6.492 ± 0.042	0.150 ± 0.002	1.297 ± 0.016	28/6
$\bar{\Lambda}$ ($\bar{u}\bar{d}\bar{s}$)	6.3	0.266 ± 0.001	21.640 ± 0.041	-0.050 ± 0.001	0.031 ± 0.001	0.2/1
	7.6	0.238 ± 0.001	25.643 ± 0.048	-0.050 ± 0.002	0.085 ± 0.001	8/3
	8.8	0.243 ± 0.001	25.502 ± 0.053	-0.050 ± 0.001	0.136 ± 0.002	7/3
	12.3	0.235 ± 0.001	25.826 ± 0.054	-0.050 ± 0.001	0.373 ± 0.005	7/3
	17.3	0.234 ± 0.002	25.826 ± 0.062	-0.050 ± 0.004	0.407 ± 0.011	40/5
Λ (uds)	6.3	0.198 ± 0.001	29.960 ± 0.038	-0.050 ± 0.001	5.570 ± 0.010	22/12
	7.6	0.200 ± 0.001	27.999 ± 0.056	-0.050 ± 0.001	6.531 ± 0.077	47/12
	8.8	0.210 ± 0.001	27.999 ± 0.052	-0.050 ± 0.003	6.165 ± 0.052	54/12
	12.3	0.222 ± 0.002	27.391 ± 0.071	-0.050 ± 0.004	5.748 ± 0.079	128/11
	17.3	0.232 ± 0.001	27.391 ± 0.064	-0.050 ± 0.005	4.354 ± 0.053	77/13
Ξ^- (dss)	6.3	0.185 ± 0.001	27.899 ± 0.057	-0.050 ± 0.002	0.432 ± 0.006	14/2
	7.6	0.187 ± 0.002	26.364 ± 0.063	-0.050 ± 0.004	0.523 ± 0.009	4/2
	8.8	0.189 ± 0.002	25.886 ± 0.062	-0.050 ± 0.004	0.521 ± 0.006	12/3
	12.3	0.203 ± 0.001	20.774 ± 0.055	-0.050 ± 0.003	0.608 ± 0.006	26/2
	17.3	0.204 ± 0.002	18.744 ± 0.064	-0.050 ± 0.003	0.661 ± 0.006	5/4
Ξ^+ (dss)	7.6	0.188 ± 0.002	26.364 ± 0.061	-0.050 ± 0.004	0.025 ± 0.001	1/-
	8.8	0.196 ± 0.002	20.062 ± 0.058	-0.050 ± 0.004	0.033 ± 0.001	2/-
	12.3	0.196 ± 0.001	20.064 ± 0.063	-0.050 ± 0.002	0.093 ± 0.001	0.2/1
	17.3	0.225 ± 0.001	17.012 ± 0.064	-0.050 ± 0.002	0.157 ± 0.002	5/2

- [11] A.N. Mishra, A. Ortiz, G. Paic, Phys. Rev. C **99**, 034911 (2019)
- [12] P. Castorina, A. Iorio, D. Lanteri, H. Satz, M. Spousta, Phys. Rev. C **101**, 054902 (2020)
- [13] ALICE Collaboration (A. Jaroslav *et al.*), Nature Phys. **13**, 535 (2017)
- [14] S. Godfrey, I. Nathan, Phys. Rev. D **32**, 189 (1985)
- [15] S. Godfrey, Phys. Rev. D **31**, 2375 (1985)
- [16] B. Szabocs, F. Zoltan, H. Christian, K. Sandor, K. Stefan, S. Kalman, Phys. Lett. B **730**, 99 (2014)
- [17] HotQCD Collaboration (A. Bazavov *et al.*), Phys. Lett. B **90**, 094503 (2014)
- [18] HAL QCD Collaboration (I. Takumi *et al.*), Phys. Lett. B **792**, 284 (2019)
- [19] HAL QCD Collaboration (S. Kenji *et al.*), Nucl. Phys. A **998**, 121737 (2020)
- [20] H. Tatsuda, Front. Phys. (Beijing) **13**, 132105 (2018)
- [21] P.-P. Yang, F.-H. Liu, R. Sahoo, Adv. High Energy Phys. **2020**, 6742578 (2020)
- [22] F.-H. Liu, Nucl. Phys. A **810**, 159 (2008)
- [23] F.-H. Liu, Y.-Q. Gao, T. Tian, B.-C. Li, Eur. Phys. J. A **50**, 94 (2014)
- [24] C. Tsallis, J. Stat. Phys. **52**, 479 (1988)
- [25] T.S. Biró, G. Purcsel, K. Ürmösy, Eur. Phys. J. A **40**, 325 (2009)
- [26] H. Zheng, L.L. Zhu, A. Bonasera, Phys. Rev. D **92**, 074009 (2015)
- [27] H. Zheng, L.L. Zhu, Adv. High Energy Phys. **2015**, 180491 (2015)
- [28] J. Cleymans, M.W. Paradza, Physics **2**, 654 (2020)
- [29] CMS Collaboration (V. Khachatryan *et al.*), JHEP **02**, 041 (2010)
- [30] CMS Collaboration (S. Chatrchyan *et al.*), Eur. Phys. J. C **72**, 2164 (2012)
- [31] CMS Collaboration (S. Chatrchyan *et al.*), Eur. Phys. J. C **74**, 2847 (2014)
- [32] CMS Collaboration (A.M. Sirunyan *et al.*), Phys. Rev. D **96**, 112003 (2017)
- [33] ALICE Collaboration (A. Betty *et al.*), Phys. Lett. B **736**, 196 (2014)
- [34] ALICE Collaboration (J. Adam *et al.*), Phys. Rev. C **95**, 064606 (2017)
- [35] CMS Collaboration (A.M. Sirunyan *et al.*), Phys. Lett. B **790**, 270 (2019)
- [36] LHCb Collaboration (R. Aaij *et al.*), Eur. Phys. J. C **72**, 2100 (2012)
- [37] PHENIX Collaboration (A. Adare *et al.*), Phys. Rev. C **88**, 024906 (2013)
- [38] PHENIX Collaboration (S. Adler *et al.*), Phys. Rev. Lett. **98**, 172302 (2007)
- [39] PHENIX Collaboration (A. Adare *et al.*), Phys. Rev. C **83**, 024909 (2011)
- [40] STAR Collaboration (J. Adam *et al.*), Phys. Lett. B **797**, 134917 (2019)
- [41] PHENIX Collaboration (S. Adler *et al.*), Phys. Rev. Lett. **91**, 072301 (2003)
- [42] STAR Collaboration (J. Adam *et al.*), Phys. Rev. C **99**, 034908 (2019)
- [43] STAR Collaboration (J. Adam *et al.*), Phys. Lett. B **797**, 134917 (2019)
- [44] ALICE Collaboration (J. Adam *et al.*), Phys. Lett. B **760**, 720 (2016)
- [45] ALICE Collaboration (D. Adamova *et al.*), Eur. Phys. J. C **77**, 389 (2017)
- [46] ALICE Collaboration (S. Acharya *et al.*), JHEP **12**, 092 (2019)
- [47] ALICE Collaboration (S. Acharya *et al.*), Phys. Lett. B **806**, 135486 (2020)
- [48] ALICE Collaboration (J. Adam *et al.*), Phys. Rev. C **93**, 034913 (2016)
- [49] ALICE Collaboration (S. Acharya *et al.*), JHEP **10**, 174 (2018)
- [50] ALICE Collaboration (S. Acharya *et al.*), Phys. Lett. B **805**, 135434 (2020)
- [51] Particle Data Group (P.A. Zyla *et al.*), Prog. Theor. Exp. Phys. **2020**, 083C01 (2020)
- [52] STAR Collaboration (B.I. Abelev *et al.*), Phys. Rev. C **75**, 064901 (2007)
- [53] G. Bíró, G.G. Barnaföldi, T.S. Biró, K. Ürmösy, A. Takács, Entropy **19**, 88 (2017)
- [54] K. Ürmösy, G.G. Barnaföldi, T.S. Biró, Phys. Lett. B **701**, 111 (2011)
- [55] K. Ürmösy, T.S. Biró, Phys. Lett. B **689**, 14 (2010)
- [56] J. Cleymans, J. Phys. Conf. Ser. **455**, 012049 (2013)
- [57] J. Cleymans, J. Phys. Conf. Ser. **779**, 012079 (2016)
- [58] J. Cleymans, G.I. Lykasov, A.S. Parvan, A.S. Sorin, O.V. Teryaev, D. Worku, Phys. Lett. B **723**, 351 (2013)
- [59] C. Wong, G. Wilk, L.J.L. Cirto, C. Tsallis, Phys. Rev. D **91**, 114027 (2015)
- [60] C. Wong, G. Wilk, L.J.L. Cirto, C. Tsallis, EPJ Web Conf. **90**, 04002 (2015)
- [61] G. Wilk, Z. Włodarczyk, Entropy **17**, 384 (2015)
- [62] J. Cleymans, D. Worku, J. Phys. G **39**, 025006 (2012)
- [63] G. Bíró, G.G. Barnaföldi, T.S. Biró, K.M. Shen, EPJ Web Conf. **171**, 14008 (2018)
- [64] K.M. Shen, G.G. Barnaföldi, T.S. Biró, Eur. Phys. J. A **55**, 126 (2019)
- [65] G. Bíró, G.G. Barnaföldi, T.S. Biró, J. Phys. G **47**, 105002 (2020)
- [66] R. Rath, A. Khuntia, R. Sahoo, J. Cleymans, J. Phys. G **47**, 055111 (2020)
- [67] S. Grigoryan, Phys. Rev. D **95**, 056021 (2017)
- [68] D. Sahu, S. Tripathy, R. Sahoo, A.R. Dash, Eur. Phys. J. A **56**, 187 (2020)
- [69] Y.-M. Tai, P.-P. Yang, F.-H. Liu, Adv. High Energy Phys. **2021**, 8832892 (2021)

- [70] R. Hagedorn, Riv Nuovo Cimento **6**(10), 1 (1983)
- [71] ALICE Collaboration (B. Abelev *et al.*), Eur. Phys. J. C **75**, 1 (2015)
- [72] ALICE Collaboration (K. Aamodt *et al.*), Phys. Lett. B **693**, 53 (2010)
- [73] A. De Falco for the ALICE Collaboration, J. Phys. G **38**, 124083 (2011)
- [74] ALICE Collaboration (B. Abelev *et al.*), Phys. Lett. B **710**, 557 (2012)
- [75] PHENIX Collaboration (A. Adare *et al.*), Phys. Rev. C **83**, 024909 (2011)
- [76] ALICE Collaboration (B. Abelev *et al.*), Phys. Lett. B **718**, 295 (2012)
- [77] I. Lakomov for the ALICE Collaboration, Nucl. Phys. A **931**, 1179 (2014)
- [78] ALICE Collaboration (B. Abelev *et al.*), Phys. Lett. B **708**, 265 (2012)
- [79] L.-L. Li, F.-H. Liu, Physics **2**, 277 (2020)
- [80] H.-R. Wei, F.-H. Liu, R. A. Lacey, J. Phys. G **43**, 125102 (2016)
- [81] H.-R. Wei, F.-H. Liu, R. A. Lacey, Eur. Phys. J. A **52**, 102 (2016)
- [82] H.-L. Lao, H.-R. Wei, F.-H. Liu, R. A. Lacey, Eur. Phys. J. A **52**, 203 (2016)
- [83] M. Waqas, F.-H. Liu, Eur. Phys. J. Plus **135**, 147 (2020)
- [84] H.-L. Lao, F.-H. Liu, B.-C. Li, M.-Y. Duan, Nucl. Sci. Tech. **29**, 82 (2018)
- [85] H.-L. Lao, F.-H. Liu, B.-C. Li, M.-Y. Duan, R. A. Lacey, Nucl. Sci. Tech. **29**, 164 (2018)
- [86] R. Sahoo, AAPPS Bull. **29**(4), 16 (2019)
- [87] NA61/SHINE Collaboration (N. Abgrall *et al.*), Eur. Phys. J. C **74**, 2794 (2014)
- [88] NA61/SHINE Collaboration (A. Aduszkiewicz *et al.*), Eur. Phys. J. C **77**, 671 (2017)
- [89] STAR Collaboration (L. Adamczyk *et al.*), Phys. Rev. C **96**, 044904 (2017)
- [90] STAR Collaboration (J. Adam *et al.*), Phys. Rev. C **102**, 034909 (2020)
- [91] NA49 Collaboration (C. Alt *et al.*), Phys. Rev. C **77**, 024903 (2008)
- [92] NA49 Collaboration (S. Afanasiev *et al.*), Phys. Rev. C **66**, 054902 (2002)
- [93] NA49 Collaboration (C. Alt *et al.*), Phys. Rev. C **77**, 064908 (2008)
- [94] NA49 Collaboration (C. Alt *et al.*), Phys. Rev. C **78**, 044907 (2008)
- [95] NA49 Collaboration (C. Alt *et al.*), Phys. Rev. C **78**, 034918 (2008)